A DEVELOPMENT OF NEURAL NETWORK MODEL FOR SPREAD-F OCCURRENCE AT CHUMPHON STATION, THAILAND

PHIMMASONE THAMMAVONGSY

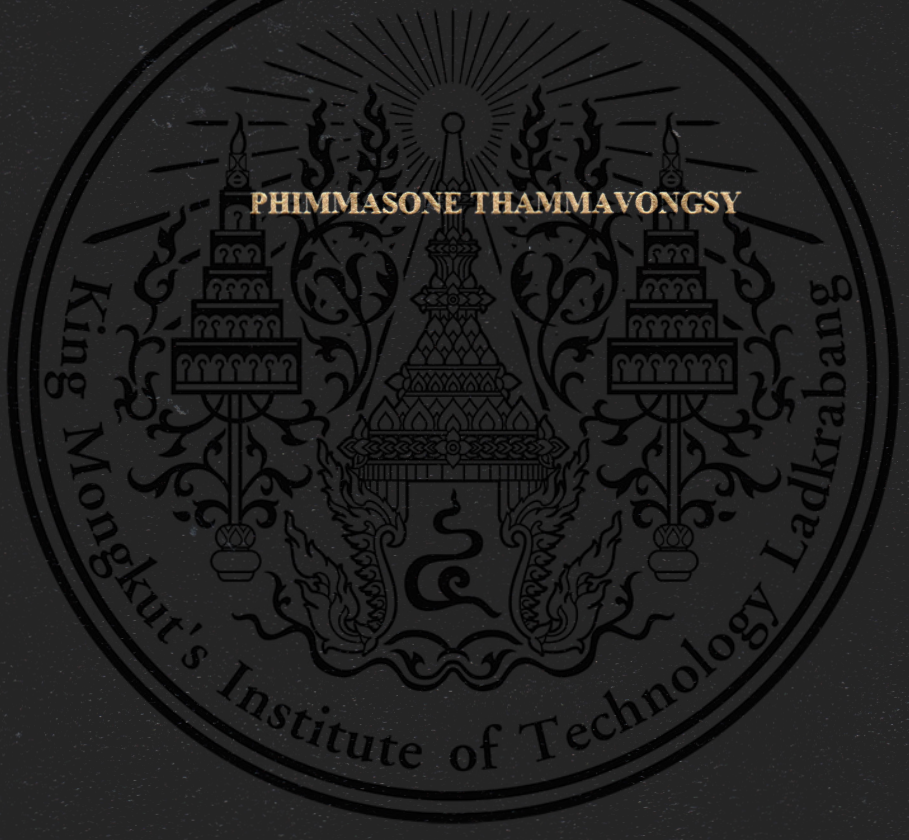

A THESIS REPORT SUBMITTED IN PARTIAL FULFILLMENT
OF THE REQUIREMENTS FOR THE DEGREE OF
MASTER OF ENGINEERING IN COMPUTING IN ENGINEERING SYSTEMS
INTERNATIONAL COLLEGE
KING MONGKUT'S INSTITUTE OF TECHNOLOGY LADKRABANG
ACADEMIC YEAR 2017
KMITL-2017-IC-M-11-03

A DEVELOPMENT OF NEURAL NETWORK MODEL FOR SPREAD-F OCCURRENCE AT CHUMPHON STATION, THAILAND

Phimmasone Thammavongsy

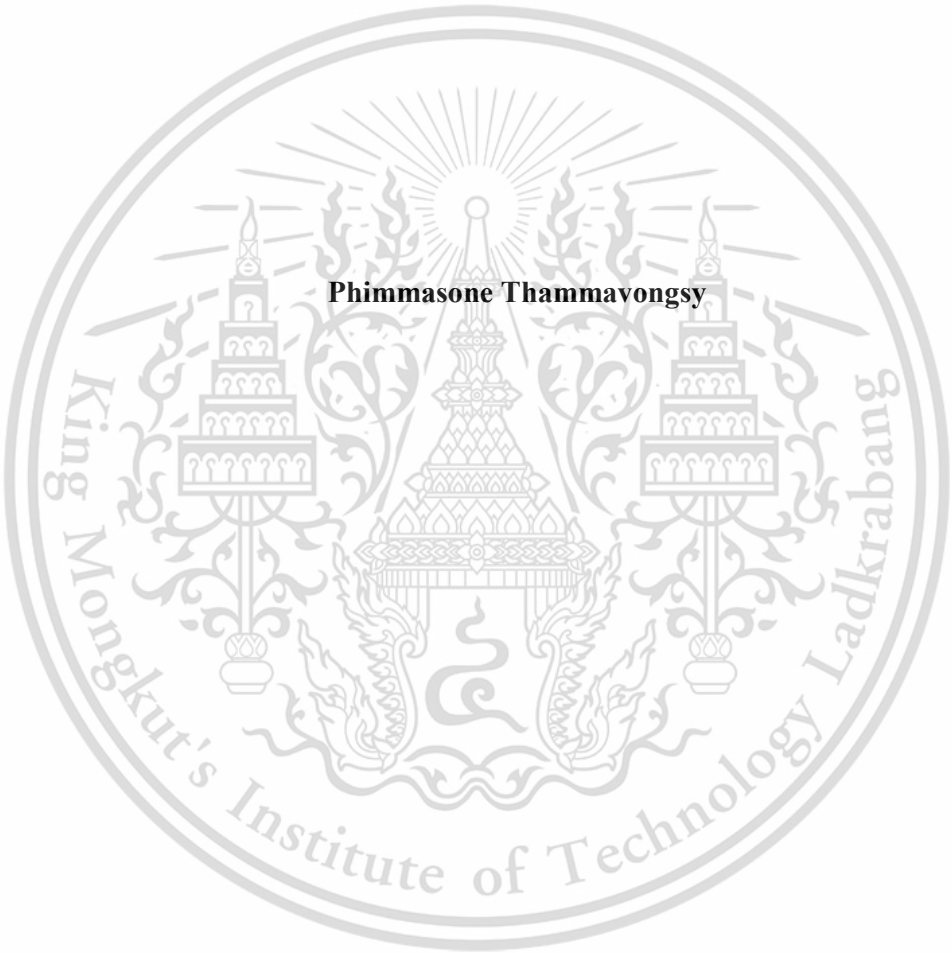

A THESIS REPORT SUBMITTED IN PARTIAL FULFILLMENT
OF THE REQUIREMENTS FOR THE DEGREE OF
MASTER OF ENGINEERING IN COMPUTING IN ENGINEERING SYSTEMS
INTERNATIONAL COLLEGE
KING MONGKUT'S INSTITUTE OF TECHNOLOGY LADKRABANG
ACADEMIC YEAR 2017
KMITL-2017-IC-M-11-03

THESIS TITLE	A Development of Neural Network Model for Spread-F Occurrence at Chumphon station, Thailand
STUDENT NAME	Mr. Phimmasone Thammavongsy
STUDENT ID	58610016
DEGREE	Master of Engineering
PROGRAME	Computing in Engineering Systems (International Program)
ADVISOR	Dr. Natthapong Jungteerapanich
CO-ADVISOR	Prof. Dr. Pornchai Supnithi

ABSTRACT

The atmospheric irregularities affect telecommunication and navigation globally, the perturbations of ionospheric layer in low latitudes near the magnetic equator have played important roles on communication systems. These ionospheric irregularities have been studied in Chumphon (CPN) area using frequency modulated continuous waves (FM/CW) ionosonde. One of the ionospheric irregularities is detected by spread-F events can be observed by FM/CW ionosonde. It is a spreading of F region in the ionosphere layer, usually occurs in the equatorial region and its appearance is detected as the traces in the ionograms. In Thailand, CPN area is in the equatorial region near the magnetic equator (latitude: 10.72°N, longitude: 99.4°E) where the ionosphere layer is strongly disturbed by the Earth's atmosphere changes. This study aims to analyze the spread-F statistics at CPN station, Thailand and develop a neural network (NN) model for predicting the spread-F occurrence based on the observed data from 2013 to 2016. As a result, this study finds that the NN model gives a satisfactory performance in prediction of spread-F event and its predicted results correspond to the measured spread-F. The model results denote the spread-F events correspond to the input parameters including time changes, seasonal changes, magnetic activity (Ap index), and solar activity (F10.7 index. Eventually, the standard deviation of the results is deviated from the actual results by approximately 20% to 30.

ACKNOWLEDGEMENT

This thesis is accomplished with the support of many people. Especially, I would like to express my deepest gratitude to my advisor Dr. Natthapong Jungteerapanich and co-advisor Prof. Dr. Pornchai Supnithi of the International College, King Mongkut's Institute of Technology Ladkrabang. Moreover, I would like to express my gratitude to AUNSEED-Net which provided scholarship for me. I appreciate the corporation of the SEALION project and National Institute of Information and Communications Technology (NICT), Japan, for supporting the equipment and technical support. Also, I am thankful to World Data Center for providing the data of solar activity and magnetic activity.

I also want to thank all lecturers for your support and guidance within the whole two years. Also, I need to express my sincere acknowledgement to Dr. Watid Phakphisut and colleagues of the Communication, Storage, Space Research Group (CSSRG) Laboratory for the encouragement and supervision. I proudly express my obligation to National University of Laos (NUOL). Finally, I must express my every greatest gratitude to my parents and all relatives for providing me with unfailing support and continuous motivation. This accomplishment would not have been possible without them.

Phimmasone Thammavongsy

TABLE OF CONTENTS

LIST OF FIGURES

LIST OF DEFINITIONS

ANN	Artificial Neural Network
Ap index	Magnetic activity
CNN	Convolutional Neural Network
COSPAR	Committee on Space Research
CSNN	Chumphon Spread-F Neural Network model
DN	Day Number
DNC	Day Number of Cosine component
DNS	Day Number of Sine component
EPB	Equatorial Plasma Bubble
ESF	Equatorial Spread-F
F10.7 index	An excellence indicator of solar activity is obtained from noise level generated at the wavelength of 10.7 cm.
FM/CW	Frequency-Modulate by Continuous-Waves propagation
foF2	Critical Frequency of F2 layer
FSF	Frequency Spread-F
GPS	Global Positioning System
HF	High Frequency
HR	Hour Number
HrC	Hour Number of Cosine component
HrS	Hour Number of Sine component
IRI	International Reference Ionosphere
LSWS	Large Scale Wave Structure
M(3000)F2	Maximum Usable Frequency reflects F2 layer in the distance of 3,000 kilometer
MSF	Mixed Spread-F
NN	Neural Network
NOAA	National Oceanic and Atmospheric Administration
PRE	Pre-reversal Electric Field Enhancement
RBFN	Radial Basis Function Network
ReLU	Rectified Linear Unit
RMSE	Root Mean Square Error
RNN	Recurrent Neural Network

RSF	Range Spread-F
RT	Rayleigh-Taylor
SEALION	South East Asia Low-Latitude Ionosphere Network
Spf_{occur}	The observed spread-F
Spf_{prob}	The probability of spread-F occurrence
SSF	Strong Spread-F
SSN	Sun Spot Number
TEC	Total Electron Content
T_{obs}	The total number of observations
Trainlm	Levenberg-Marquardt training algorithm
URSI	International Union of Radio Science

CHAPTER 1
INTRODUCTION

1.1 Motivation

The ionospheric irregularity is a primary inspiration to make this research. It is mainly caused by the plasma density variations which rapidly occur across the geomagnetic field. The scale length of ionospheric irregularities can range from a few meters to several kilometers across the magnetic field and its influence plays an important role in satellite communication systems [1]. The appearance of F region irregularities often occurs in the nighttime as often called spread-F, which is derived from spread of ionogram trace on ionogram data when this irregularity occurred. In previous works, the ionosphere irregularity is studied, and its appearances can be detected by the FM/CW ionosonde [2] [3]. The study of probabilities of spread-F occurrence has been investigated in terms of statistical analysis and forecasting model. Such a global spread-F model has been presented by the International Reference Ionosphere (IRI) model supported from the Committee on Space Research (COSPAR) and the International Union of Radio Science (URSI) [4]. The published study of the forecast model for estimating the probabilities of spread-F occurrence was presented over Brazilian region using neural network (NN) in 2010 [5]. The machine learning method called artificial neural network is familiar as a popular method for computational intelligence. In 2014, the artificial neural network (ANN) was applied to create the prediction model of critical frequency of F2 layer (foF2) in Chumphon (CPN) station, Thailand [6]. Similarly, the NN is applied to predict the total electron content (TEC) in equatorial latitude station in Thailand [7]. The near-real time foF2 predictions was presented for the development of a near-real time global foF2 empirical model using NN [8]. Development of an ANN models for forecasting the global solar radiation in AI Ain City - UAE by using MATLAB is presented [9]. The ANN has been effectively used to solve the variety of problem, especially, in terms of the natural phenomenon and space variations. All the things considered, this thesis proposes the development of prediction model for predicting the probabilities of spread-F occurrence in CPN station near the magnetic equator, Thailand.

The equatorial spread-F is at earliest time detected by an ionosonde from the study of F region ionosphere-investigations at low latitudes [10]. The influences of equatorial spread-F affect the radio wave communication system such as the navigation

system and radio wave propagation [11]. The occurrence of equatorial spread-F mostly occurs at night time which begins after sunset until before sunrise in low latitudes. The equatorial spread-F types were seen on an ionogram of ionosonde; they were categorized into various types as their spreading characteristics such as frequency spread-F (FSF), range spread-F (RSF), mixed spread-F (MSF) and strong spread-F (SSF). The range spread-F is one of these spread types which are believed to associate with the development of the plasma bubble events [12]. The development of equatorial spread-F processes was well described in the theory of the Rayleigh-Taylor instability [13]. The equatorial spread-F (ESF) is the equatorial irregularities in F region which particularly occurs in low latitudes near the magnetic equator. Thus, the most studies of ESF have been noticed in the equatorial region more than other regions and an equatorial region plays a very important role for investigating the spread-F irregularity. Then this thesis focuses on range spread-F causing its strong influences impact on trans-ionospheric radio-wave communication.

1.2 Thesis objectives

The major objective of this thesis aims to develop a neural network-based model for predicting the probabilities of spread-F occurrence of a single model in CPN station. Moreover, this thesis includes are composed of the study of spread-F phenomenon, specifically the cause and the significant effects and its variability. The intention is to come up with a suitable input space for the NN model. This thesis also explains the principle of NN modelling techniques which are utilized in this development of spread-F model.

1.3 Scope of the study

This study is limited by the availability of dataset. The spread-F data available from CPN station covers the period of four years from 2013 to 2016. Hence, the chosen datasets for training the network model is gained from 2013 to 2015. The considered inputs of this network model are composed of the seasonal variations, diurnal variations, solar activity represented by F10.7 index and the magnetic activity denoted by Ap index. The learning process of network model is trained by applying the backpropagation algorithm and the random selection is applied to split datasets into set of training and test for training the network model. The trained network model is tested with the new input (unknown) data in 2016 for validating the efficiency of network model. The performance of network model is examinable by considering the root mean

square error (RMSE) between the desired output and the actual output. Lastly, the results of network model are performed as results in 2016 which are compared between the predicted values and observed values. The comparison of these two results is to validate the network model's accuracy.

1.4 Thesis overview

This thesis consists of six chapters. Chapter 1 presents the aims and outlines of this research. Chapter 2 provides the theoretical background of spread-F and its variability and gives some ionogram images illustrating the presence of different types of spread-F. Chapter 3 presents a brief introduction to the basic literature on the neural network technique as used in this study. Chapter 4 describes the determination technique of spread-F NN model and the data sources, the determination shows an initial attempt to determine the optimum parameters for the input space for CPN neural network model and performs the determination of hidden layer as an optimum. In Chapter 5, the obtained results from the NN model and observations are presented and discussed. The network model's performance is evidently validated with the observed results and moreover, an error analysis is performed for analyzing some cases when the Chumphon spread-F NN (CSNN) model does not perform very well. A comparative analysis of the CSNN model results and the observed results are demonstrated and discussed in selected months in 2016. The conclusions of this study are summarized in Chapter 6.

CHAPTER 2
IONOSPHERIC DISTURBANCE AND SPREAD-F EVENTS

2.1 Introduction

This chapter presents the literature reviews on an ionospheric disturbance and the spread-F phenomenon near an equatorial region. The variability of equatorial spread-F is based on various factors. The irregularity of equatorial region connecting the generation of range spread-F (RSF) event which is associated with the development of plasma bubble events.

2.2 The spread-F phenomenon

The spread-F phenomenon is an event within the ionospheric layer which is often mentioned whether its occurrence is due to the reshape of F layer after sunset. As shown in Figure 2.1, the atmospheric structure can be neatly organized by a representative temperature profile and while the ionosphere is more sensibly organized by the number density of the plasma. Let us look at the ionized Gas, this increase is due primarily to the absorption, by ozone, a part of the ultraviolet portion of the solar radiation [14].

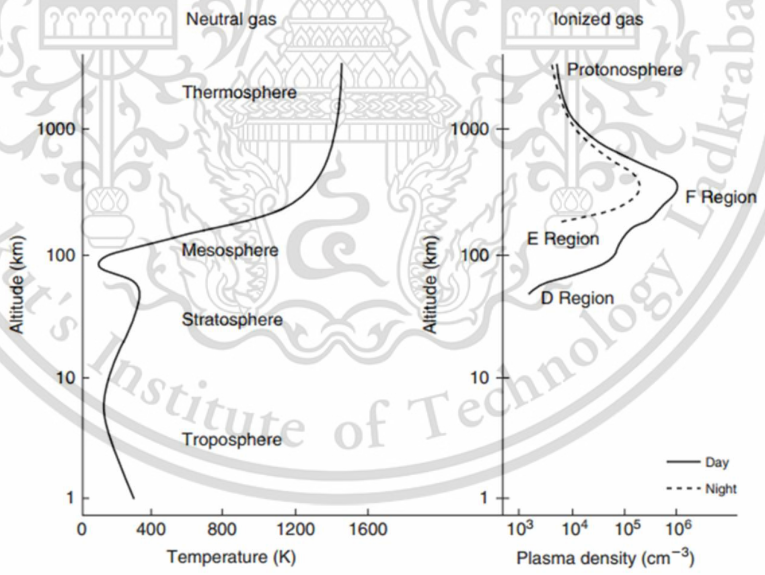

Figure 2.1 The profiles of neutral atmospheric temperature and ionospheric plasma density with the various layers designated [14].

Basically, the earth's ionosphere layer is a partially ionized gas which surround the earth in the altitude range 90- 1000's kilometer. Hence, when the electromagnetic waves propagating through the ionosphere can be impacted in terms of a phase and

amplitude fluctuations, absorption, scattering, frequency shifts, etc. Moreover, the degradation of magnetic radiation can impact the communication and the navigation systems [15]. The equatorial ionospheric layer has been become extremely disturbance after sunset because of a phenomenon of equatorial spread-F [16].

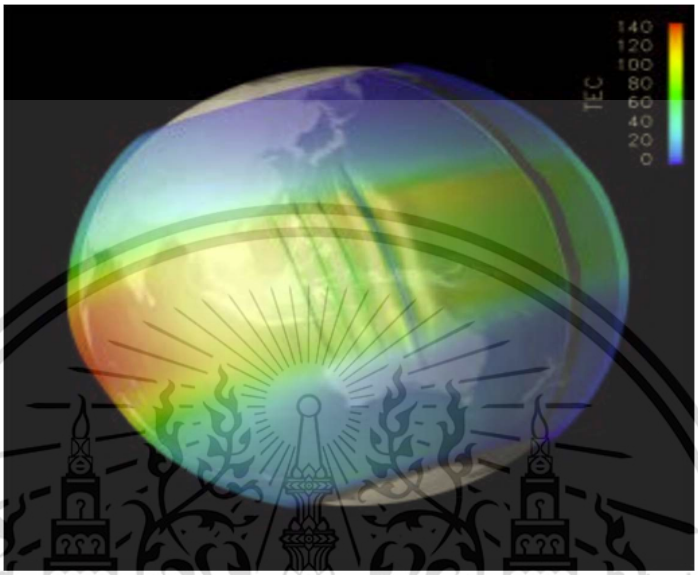

Figure 2.2 The 3D graphic of TEC showing the impact of equatorial spread-F in the equatorial region [16].

The occurrence of plasma instability phenomena in the equatorial spread F region of ionosphere are usually combined under the generic name so called equatorial spread-F (ESF). The ESF events are firstly detected by using an ionosonde [10], which showed that the reflected echo was spread out in either range or frequency due to the multiple reflection paths created by the turbulent ionosphere. This phenomenon occurs primarily at night time in ionospheric layer in the equatorial region. The plasma instabilities in ESF occur on time scales ranging from seconds to hours and length scales from tens of centimeters to hundreds of kilometers [15]. The ESF perturbation is developed by a complex process which consist of many electrodynamic mechanisms. The development of ESF is mainly generated through the gravitational Rayleigh – Taylor (R-T) instability mechanism in conjunction, which is mainly driven by the evening pre-reversal electric field enhancement (PRE) causing a rapid uplift of equatorial F layer [17]. Therefore, the appearance of ESF events are a variation process of plasma density in an ionospheric layer which almost occur after sunset to pre-sunrise.

2.2.1 Variations of equatorial ionosphere

The equatorial ionospheric layer is the region where the Earth's magnetic field line is nearly horizontal. The highest plasma density is discovered in the ionospheric layer closer to the equatorial region, thus, this region is especially important to be studied as its influences cause the equatorial anomaly that impact the wave propagation system and navigation system [11]. The equatorial anomaly is interpreted by the fountain effect, that is, the vertical electrodynamic drift at the equator and plasma diffusion away from the equator along the geomagnetic field lines. As shown in Figure 2.3, the fountain effect is caused by the upward drift of electrons under the merged influence of horizontal electric and magnetic fields, then the spread down along lines of force of the Earth's magnetic field towards altitudes and higher latitudes [18].

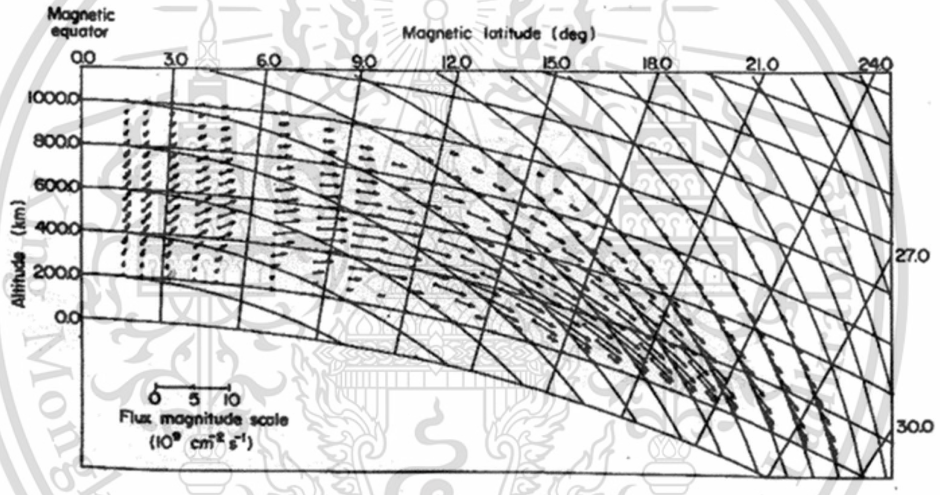

Figure 2.3 The fountain effects [18]

The ambient ionospheric plasma gradient is both antiparallel (parallel but oppositely directed) to gravity and perpendicular to the magnetic field, coupled with the east – west electric field. This physical arrangement is unstable to small bottom side plasma density perturbations.

2.2.2 The Rayleigh – Taylor instability

The Rayleigh – Taylor instability or RT instability is a more powerful explanation of an instability of an interface between two fluids of different densities when the lighter fluid is being pushed the heavier fluid such as the behavior of water suspended above oil in the gravity of Earth [19]. A heavy fluid is pushed by light fluid, it is called a dynamic process whereby the two fluids seek to reduce their combined

potential energy [13]. The movement of the force of gravity on the electrons and ions causes them to drift parallel to the boundary [20]. In more details, a perturbation of the interface between the fluids causes the plasma density to make the sinusoidal variations in the *z* direction as shown in Figure 2.2, the magnetic field points out of the paper. The ion and electron boundaries are separated out by drifting and this gives an upward movement to the electric fields as denoted on the left in Figure 2.4. In that case, an ExB drift is produced in the opposite direction amplifying the initial perturbation [21].

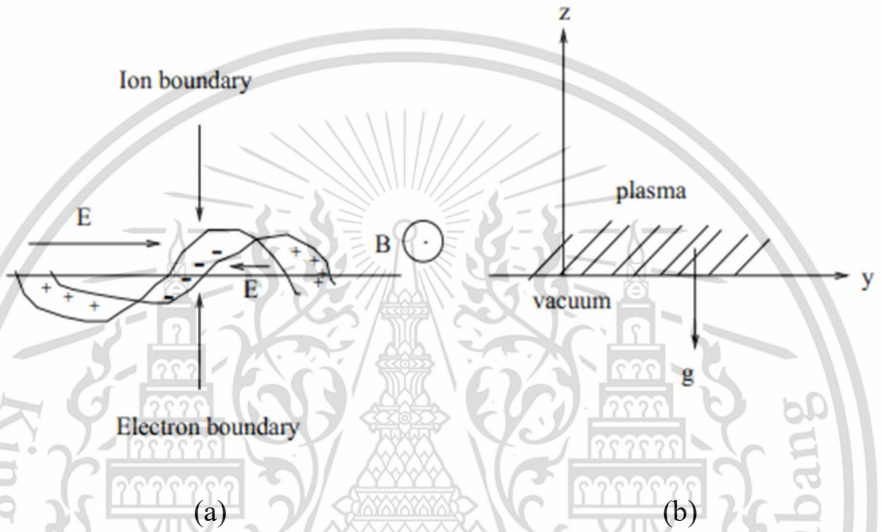

Figure 2.4 Rayleigh – Taylor instability schematic diagram [20].

When the gravity waves are propagated perpendicularly to the magnetic field, they generate a polarization electric field, and these are amplified by the R-T instability [22]. Thus, the plasma fluid equations of continuity, motion, and current continuity can be combined to provide the local linear growth rate for instabilities. The linear growth rate can be estimated by the local linear growth rate γ of the collisional R-T instability [23]. It is expressed as

$$\gamma = \frac{\partial n}{\partial h}\frac{1}{n_0}\frac{g}{v} - R \qquad (2.1)$$

where n_0 is the background electron density, h is the altitude above the Earth's surface, v is the ion-neutral collision frequency, g is gravity (positive downward), and R is the local recombination rate.

The above expression provides that the fundamental ionospheric conditions necessary for the ESF occurrence. The growth rate γ is at the greatest level when the

height of ionospheric layer is enhanced, maximized the g/v term when the bottom side density gradient is sharped, and this event usually occurs after local sunset. Hence, the day-to-day variability of ESF may be related to the atmospheric effects like the gravity waves that can trigger the R-T instability during the trans equatorial thermosphere winds tend to impede the development of instability [24].

2.3 The characteristics of spread-F

The equatorial spread-F (ESF) irregularities frequently occur in the low latitudes near magnetic equator regions. The variability of ESF can be observed at night time during 18:00LT and 06:45LT as a characteristic doubling of F region and the increase of virtual height of F layer. In term of spread-F is coined to describe the unusual F trace in ionogram data, namely, the FMCW ionosonde attempts to measure the reflection of radio waves depending on each height of F layer while the instability process is occurring in the F layer of ionosphere. The result of ionogram echo trace is spread out along the range and frequency axis causing the multiple reflection paths of the radio waves. Then spread-F in equatorial region can be categorized as the dissimilar spread of ionogram trace. The types of spread-F are defined by spreading of ionogram trace comprising frequency spread-F (FSF), range spread-F (RSF), mixed spread-F (MSF) and strong spread-F (SSF) as shown in Figure 2.5.

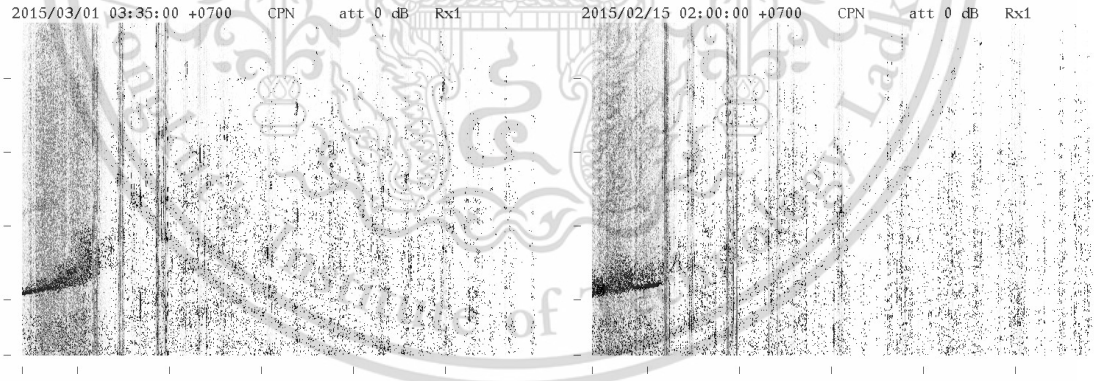

(a) frequency spread-F (b) range spread-F

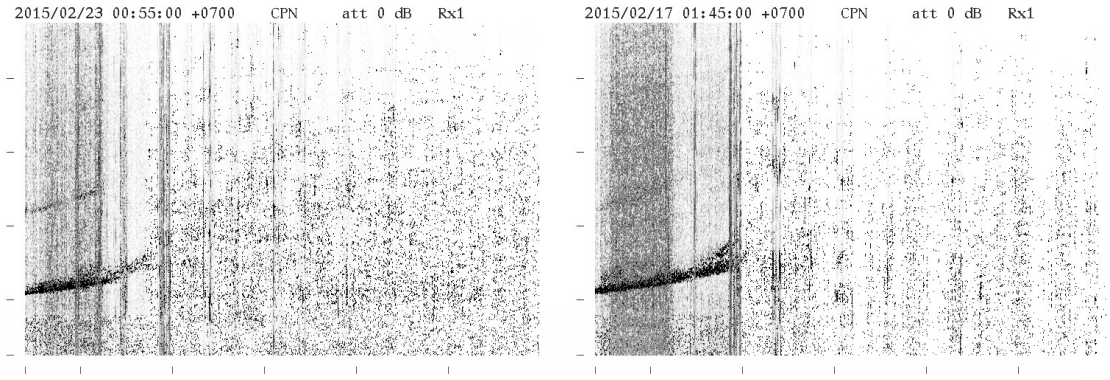

(c) mixed spread-F (d) strong spread-F

Figure 2.5 The equatorial spread-F types in an ionogram data from Chumphon station.

The ionogram format is determined as the figure format by preprocessing the received HF echo from reflection, where the horizontal axis represents the frequency range of 2 – 30 MHz and the altitude of ionosphere is along the vertical axis extending from 1 – 1,000 kilometers above the Earth's surface. Therefore, the classification of each spread-F type depends on the spread of F trace which appears on an ionogram in Figure 2.5(a) – 2.5(d).

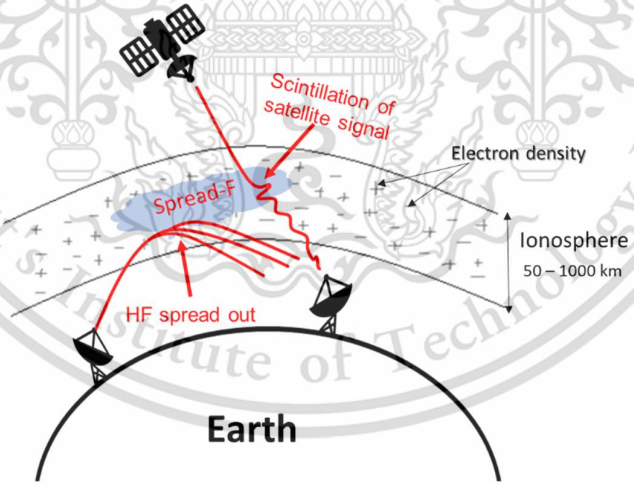

Figure 2.6 Spread-F impacts on radio wave propagation.

2.3.1 Frequency spread-F (FSF)

This spread type is so called FSF as the signature of which typically shows an echo wide spread along the frequency axis near the critical frequencies of the ordinary and extraordinary traces of the ionograms and, therefore, FSF is associated with the

high frequency irregularities close to the F peak region. The appearance of FSF can impact on the narrow band spectrum near the peak of F region [15].

2.3.2 Range spread-F (RSF)

The characteristic of this spread F region is indicated by the signatures of which are characterized by an echo widespread along the height axis. This spread-F type is the processes in the plasma irregularities in the lower part of the F region and, moreover, it plays a significant role on the association with plasma bubbles which are the main issue on the propagation of the HF radio waves in the communication systems and navigation system [22]. This type of RSF is more seen in CPN station.

2.3.2.1 Association of range spread-F with EPB

An equatorial spread-F perturbation is believed to associate with the various irregularity phenomenon. Particularly, the range type spread-F (RSF) is referred whether it associates to the development of plasma bubble events. RSF becomes the disturbance factor indicating the irregularity of narrow spectrum that occurs near the peak of the F layer is not due to instability or potentially unstable and flux tubes [12]. Thus, the spread-F is detected by radiating a short pulse of high frequency radio waves upward, these waves are reflected by the ionosphere at different heights depending on plasma density and the result of reflected waves are preprocessed and performed as traces in the ionogram. As illustrated in Figure 2.7, spread-F can be specifically observed by the appeared trace in the ionogram. The purpose of this study, the spread-F presence is assigned by “1” and spread-F absence is represented by “0”.

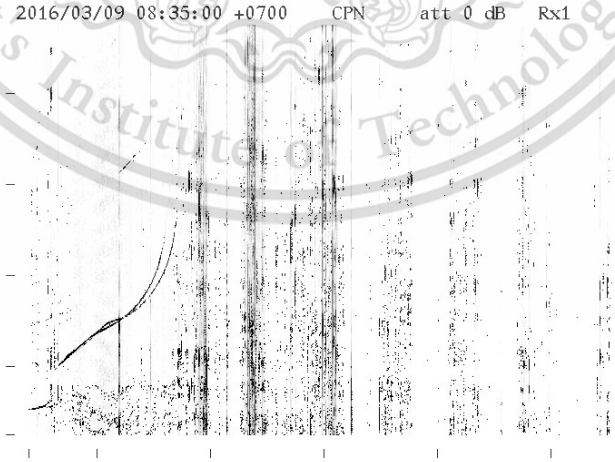

Figure 2.7 The appearance of F layer traces without range spread-F.

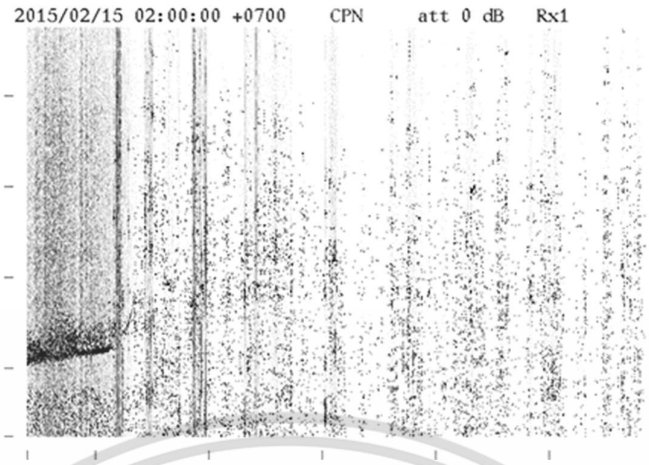

Figure 2.8 The appearance of F layer trace is caused from the presence of RSF.

2.3.3 Mixed spread-F (MSF)

This spread of F trace is a combination between FSF and RSF. The signatures of which typically display an echo widespread cover both frequency axis and height axis of the ionograms as shown in Figure 2.5(c). This spread type is especially defined as RSF type in some case depending on determination of researches. Then the effect of MSF is mostly same as FSF and RSF.

2.3.4 Strong spread-F(SSF)

SSF is very similar to RSF and MSF in term of spreading shape. The signatures of which are characterized by a large echo widespread along the height axis and long widespread along frequency axis. Then this typical spread-F is defined as same as the typical RSF causing its influence and spread shaped are similar with RSF.

According to the effectiveness of spread-F, whenever either of the spread-F is appeared the radio wave propagation is disturbed, its influence affects the other ionospheric parameters, for example, foF2 and M(3000)F2. That means the occurrence of spread-F impacts on ionospheric parameters, those ionospheric parameters cannot be scaled due to the spread out of F trace. Consequently, these spread-Fs maybe differently specified by the researchers in scaling of spread-F values, this thesis defines each typical spread-F using the letters such as the frequency spread-F is indicated by *"F"*, range spread-F is represented by *"R"*, a letter *"M"* is assigned to mixed spread-F and *"S"* for strong spread-F. These representative letters describe that each particular letter of spread-F is translated or changed to the different number as the different type of spread-F in the real utilization of spread-F.

2.4 Equatorial spread-F

The equatorial spread-F event can be often seen in equatorial ionospheric layer during post sunset to before sunrise due to the fluctuation of plasma density in ionospheric layer. Variability of ESF is naturally varied from day-to-day and it can be evidentially visualized by variety of variabilities including the diurnal variations, seasonal variations, solar cycle, latitude, longitude, magnetic activity and geomagnetic activity. ESF is mostly observed in low latitudes or equatorial regions than higher latitudes. For instance, the study of ESF is investigated as longitude sectors and the characteristics of ESF in different latitudes are studied in Southeast Asia [25, 26]. Hence, an understanding of spread-F variations leads to the significant parameters that must be considered for designing the neural network inputs.

2.4.1 Seasonal variations of ESF

The Earth's rotation around the sun is differently defined for each season. The ESF occurrence statistics are acceptably related with seasonal variations. In equinoctial months and solstice months, the ESF more often occurs in the equinox than solstice in low latitude region [27]. Therefore, the variability of ESF is seasonally controlled and its occurrences are approximately caused by this condition when the sun position is vertically above the observatory in the equinox season.

2.4.2 Diurnal variations of ESF

The diurnal variations refer the Earth's rotation around itself over each period of a day, hence, the cycle of time be relatedly visualized in the irregularities of plasma density at each time. The magnetic field lines are mapped to the lower and higher latitudes in equatorial F region. After sunset, the conductivity of E region is dropped, and the electric fields are produced at the bottom side of the F region that can drive the plasma instabilities. Thus, the ionospheric plasma irregularities are possibly caused by the rapid uplifting of the F region at night time.

2.4.3 F10.7 cm radio emission with ESF events

The F10.7 index is one of the longest running records of solar activity with radio wave length at 10.7 cm (2800 MHz). The F10.7 is an excellent indicator of solar activity from the noise level which is generated by radiating from the sun at the wavelength of 10.7 cm. This index correlates with the sunspot number as well as the number of Ultra Violet (UV) and visible solar irradiance records [28]. The irregularities of equatorial F region are mentioned that fluctuations of F region are due to the ionization from the

solar radiation. As the correlation of F10.7 index with solar activity, it is successfully used in the study of the Brazilian spread-F model with a sun spot number as well as in this thesis [29].

2.4.4 Magnetic activity (Ap index) associates ESF change

In equatorial region, the ionosphere irregularity is more often mentioned that it receives the disturbance from the influence of geomagnetic field so called the geomagnetic storm which can be indicated by observing the value of Ap index and Kp index. Ap index is widely utilized to describe the variations of geomagnetic field that is acquired from computing an 8-point running average of successive 3-hour Ap indices during a geomagnetic storm event and is uniquely associated with the storm event [28]. Therefore, Ap index is an indicator of magnetic field variations that is selected to be a space input of the NN input parameters.

2.5 Equatorial plasma bubbles

Ionospheric irregularity phenomenon near the Earth's magnetic equator line is called an equatorial plasma bubble which can strongly impact the radio waves propagation and the performance of GPS. The radio waves are passed through this plasma bubble are weighted as the time so called the delay time of signal. The plasma bubble event is studied and denoted whether it associated with spread-F [21]. After sunset at the equatorial region, the movement of F layer is raised up during the enhanced eastward electric field resulting from the recombination processes of F layers. At period of ESF event, the high plasma density magnetic flux tubes at the bottom side of F layer moved to the other places with lower density flux tubes from below that is analogous to the hydrodynamic R-T instability.

The pre-reversal enhancement of eastward electric fields moves the F layer to a higher and more unstable altitude. The variability of ESF is changed from time to time results because of perturbation in the electric field strength and the parameters of gravity waves, such as amplitude, frequency and wave length. ESF is interpreted as plasma density irregularities associated with EPBs that nonlinearly evolved into the topside ionosphere. Numerical simulations have been powerful tool to study the fully non-linear evolution of EPBs, which cannot be wholly understood from theoretical prediction. The equatorial plasma bubbles have been successfully simulated by three-dimensional HIRB model [30].

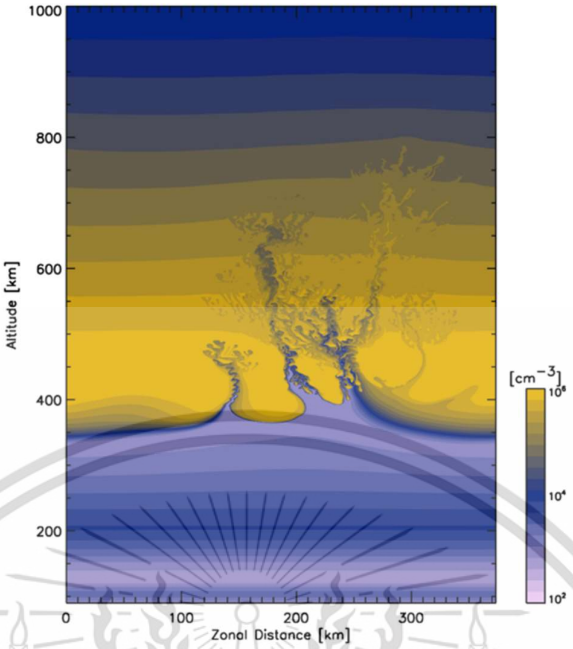

Figure 2.9 The ESBs simulated by three-dimensional HIRB model [30].

Figure 2.9 shows the 2-D snapshot of the higher simulation of ESBs as zonal plasma during the growth phase of large-scale wave structure (LSWS or so-called a hundred kilometers-scale upwelling of the bottom side of the F region) upwelling [31]. The plasma bubble is uplifted from >200 km to < 1,000 km causing the plasma density irregularities in the F region. While the plasma bubble is being developed, the increased height of F region is evidently seen. The upward of plasma bubbles is driven by the Rayleigh – Taylor instability as shown in Figure 2.10.

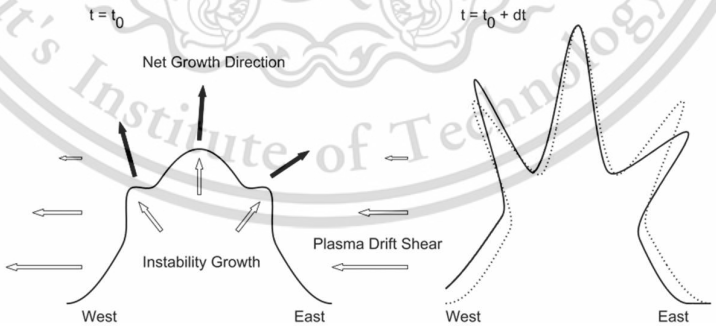

Figure 2.10 A schematic view of the east-west mechanism [31].

In Figure 2.10, solid curves represent the density contour and the dotted curve is a symmetric growth of the initial seeding without plasma drift shear. The large-scale wave structure (LSWS) upwelling and small-scale seedings at the beginning phase is expressed in the left contour. The symmetric density perturbation is only considered,

the instability growth (upward/outward) driven by the Rayleigh – Taylor instability should also be symmetric (upward white arrows). Having a vertical shear of westward plasma drift (horizontal white arrows), the lower part of the density contour shifts to west so that a relative net growth direction at the top of the upwelling leans toward the east (black arrows). Accordingly, the growth speed of the seeding at the west wall is faster than that at the wall as shown in the Figure 2.10 (right). Then the asymmetry is formed at the bottom side of the F region before the seeding fully developed as EPBs [31].

2.6 Summary

The background theory of spread-F events and plasma bubble are briefly presented. Also, an equatorial ionosphere perturbation is due to irregularity of ionospheric region near the magnetic equator region as mentioned. Moreover, the additional details on the spread-F phenomenon can be seen in the references as provided in this chapter.

CHAPTER 3
NEURAL NETWORKS

3.1 Introduction

This chapter presents the background theory of neural networks and the applied approach to determine the neural network architecture and the neural network parameters. Especially, the implementation of neural networks on MATLAB is presented and discussed in this chapter.

3.2 An artificial neural network

A popular method of machine learning is called an artificial neural network (ANN) which is widely mentioned and utilized as a tool for a specific application such as pattern recognition or data classification through a learning process. The NN is a massively parallel distributed processor made up of simple processing units that a natural propensity is designed for storing experimental knowledge and making it available in utilization as illustrated in Figure 3.1. Recently, the new ideal is called the "information bottleneck" which is presented in Qauntamagzine helping to explain the success of today's artificial intelligence algorithms and explain how human brains learn [32].

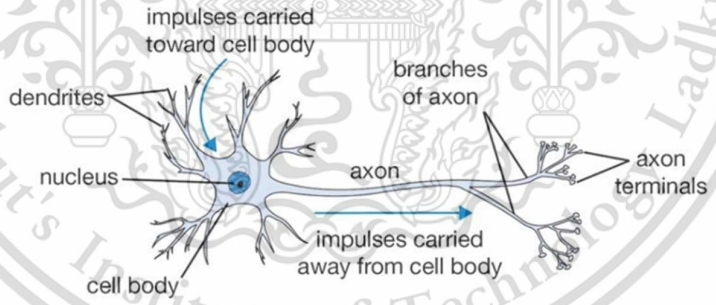

Figure 3.1 Biological neural within human brains [33].

The ANN is modeled by following the biological neural as shown in Figure 3.2. Scientist used the mathematical model to indicate how the ANN works on the concept of biological neural of human brain as illustrated in Figure 3.3. The network operation is based on behaviors of flow impulses in biological neuron as shown in the mathematical model.

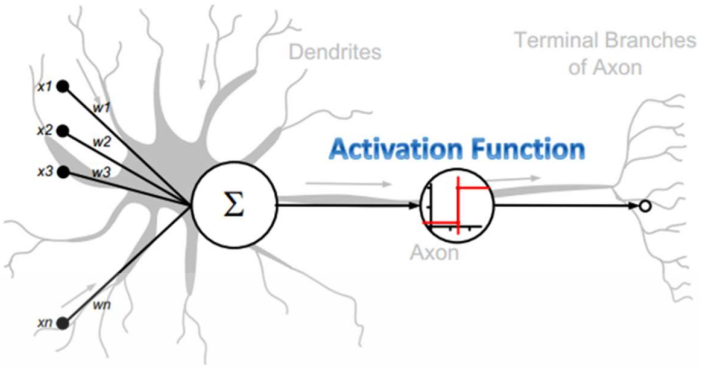

Figure 3.2 Artificial neural networks [33].

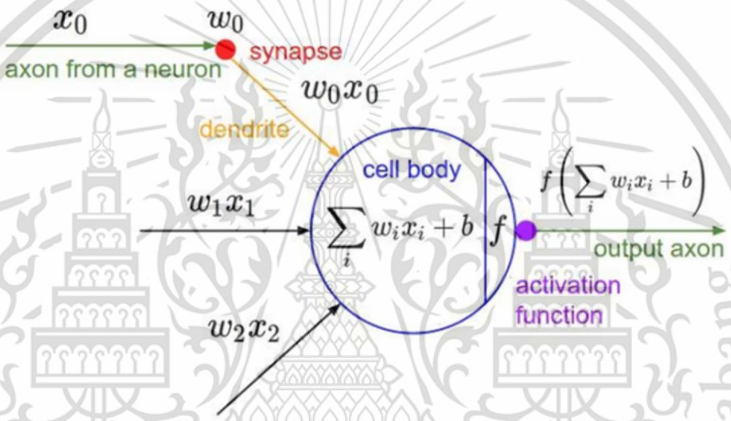

Figure 3.3 Mathematical model [33].

The complexity of artificial neural network is simply achieved by Rosenblatt's perceptron, it is the first algorithmically described about the ANN [34]. ANNs have been successfully applied in speech production, pattern recognition, control system and business by [35]. Currently, the NN can be simply implemented in several programing languages. In this study, the neural network model is mainly implemented in Matlab.

3.2.1 Supervised and unsupervised learning algorithms

The machine learning can be taught by these two learning algorithms. The learning methods in adaptive networks can be classified into two categories, namely, the supervised and unsupervised learning. Supervised learning can be achieved by presenting a sequence of training vectors that is involved with the output target vector, that means the training data includes both the input and the desired results or targets. For example, the correct results are known and provided in input to the model during the learning process. These methods are usually fast and accurate. The weights are

adjusted such the learning algorithm. For unsupervised learning, the network model is self-organized by grouping the similar input vectors together as the same class without the use of training data to specify what a typical member of each group looks like, namely, the model is not provided with the correct results during the training. The weights are updated in such a manner that the most similar input vectors are assigned to the same output unit. It can be powerfully utilized to cluster the input data in classes based on their statistical properties only. Therefore, the learning method of NN model works on supervised learning algorithm, it is a backpropagation algorithm in this thesis.

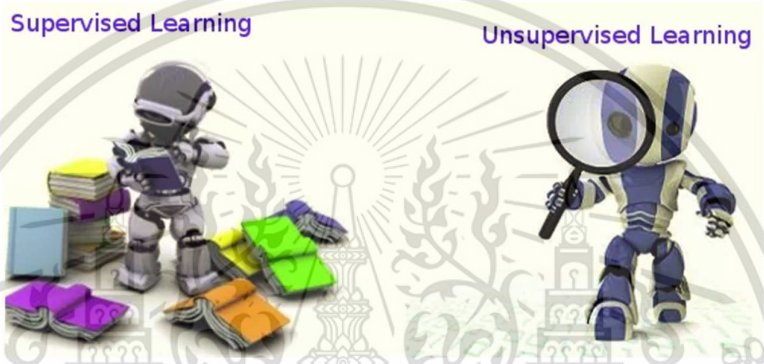

(a) (b)

Figure 3.4 (a). Supervised learning and (b). Unsupervised learning [36].

There are several training algorithms are proposed in NNs. For example, the twelve training algorithms are tested for selecting the appropriate backpropagation training algorithm in data pattern recognition, its experiment results are confirmed that the training method of Levenberg-Marquardt (trainlm) provided the highest accuracy [37]. Then the Levenberg-Marguardt training algorithm is selected to train the NN model in this study.

3.2.2 Neural network model

NN models have been globally proposed by many works. The determination of NNs are variously designed, basically, the architecture of NN is consisted of three main layers such as the first layer so called the input layer, following by the hidden layers, and the output layer. All these neural network layers correspond to the concept of human brain system as presented. Hence, the information processing of NN is computationally operated in each neuron unit that is contained in each layer as illustrated in Figure 3.2. All neuron units are connected to other units by weights; each

input is summed up together at middle neuron or hidden neuron and the output must be passed through an activation function before producing result at the output layer.

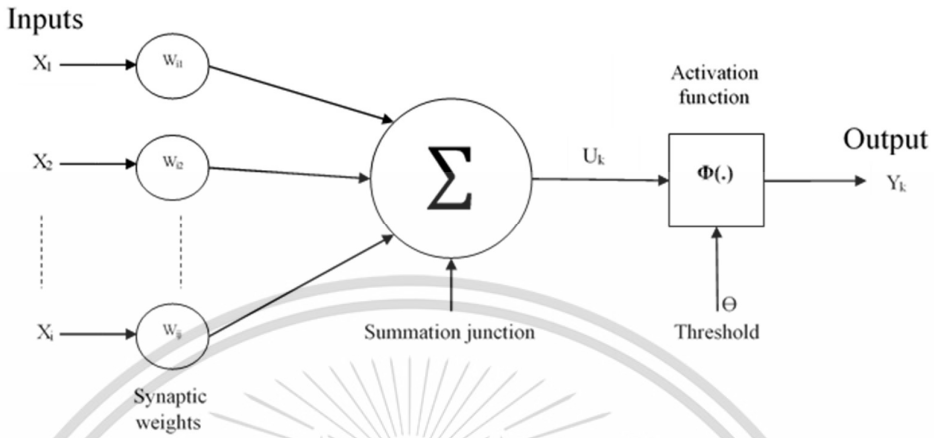

Figure 3.5 A generic neural network model.

Figure 3.2 shows a fundamental of NN model for a nonlinear model, where X_i is an input signal at the inputs of synapse *p (p = 1, 2, 3..., i)* connected to a neuron *j* and it is multiplied by the synaptic weights W_{ij}. The weight values can be either the positive or negative values [38]. The amount of weight signals is summed up by the combiner in junction at the hidden layer. The output signal amplitude is limited in the specified range by the activation function *Φ(.)* and the threshold is to increase or decrease the net input of the activation function.

Usually, an activation function is a non-linear function including the binary threshold function, bipolar threshold function and a sigmoid function. The sigmoid activation function is applied in this NN model as

$$f(x) = \frac{1}{1+e^{-\alpha x}}, \tag{3.1}$$

where *f(x)* is a sigmoid function and α is a slope parameter of sigmoid function. This activation function is both differentiable and continuous that is an appropriate activation function for a backpropagation algorithm.

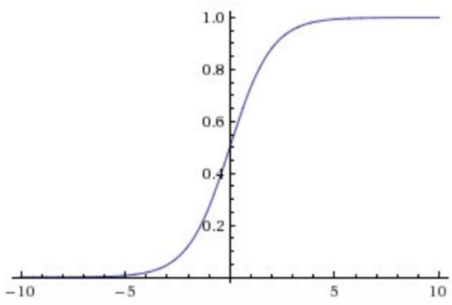

Figure 3.6 Sigmoid non-linearity with range between 0 and 1.

3.2.3 Neural network architecture

Recently, the machine learning plays a significant role in global utilizations and it is widely used in several engineering fields. The background infrastructures of neural network design depend on three main layers including input layer, hidden layer and output layer.

3.2.3.1 Input layers

The input layers include more than one input signal which depend on the input's attributes as determination. For example, there are six input signals that their attributes are investigated to associate with spread-F event, for instance, the seasonal variations (DNS and DNC), diurnal variations (HrS and HrC), solar activity (F10.7 index) and magnetic activity (Ap index). The day number represents the variability of season by cyclic components of sine and cosine. Also, variability of time is computed as hour number in cyclic component. F10.7 index represents the effects of solar radiation on radio wave frequency, and Ap index describes the variability of Earth's magnetic field. Then, these six input parameters are determined to be the NN input parameters based on their relationship with spread-F event [29] [8] [39] [7] [6].

3.2.3.2 Hidden layers

The number of hidden layers and nodes are carefully evaluated by the performance of NN model after training. Therefore, the hidden layer and neuron are repeatedly implemented in several times for seeking the optimum value that can reduce the overfitting and underfitting of training of NN model. The hidden layer is responsible for connecting between the input and output layers based on the weight values. In additions, all input signals from the input layer to hidden layer are multiplied with weight values at each connection point from layer to layer and their input signals are

summed up at the hidden layer before transferring toward to the output layer as shown in Figure 3.2.

3.2.3.3 Output layer

According to the characteristics of spread-F, it is conditionally categorized by a binary as its occurrence, namely, spread-F presence is represented by a "1" and spread-F absence is represented by a "0". Thus, the output layer is divided into two classes based on spread-F presence and spread-F absence. The final layer of NN model so called the output layer corresponds to the desired results. The weight connections are randomly given in NN model; we applied the backpropagation algorithm to train the NN model. When the training epoch reaches a given iteration and the error is computed and propagated back to the input layer order to minimize the error of network or updating weight values at each connection [38].

3.3 Types of artificial neural networks

Currently, there are several kinds of ANN. The NNs are implemented as the mathematical operations and a set of required parameters to produce the desired outputs. Hence, below are the brief details of some types of NNs which is popularly seen recently.

3.3.1 Feed forward neural networks

The simplest type of ANN is called the feed forward neural networks (FFNN). This typical NN has been used to solve several issues. Additionally, the learning of NN model is also more important and the one of powerful learning methods is called a backpropagation algorithm which mathematically works on gradient descent method. This method can be globally noticed in training the NN model. It works on the principle of minimizing the total squared error of the obtained output. Therefore, we defined the FFNN with the multi hidden layers by adjusting serval number of hidden layers. Our NN model is trained with the backpropagation algorithm. As shown in Figure 3.3, each neuron in a layer has only direct connections to the neurons of the next layer. All inputs i are linked to all neurons of hidden layer h and the output neurons are given by Ω.

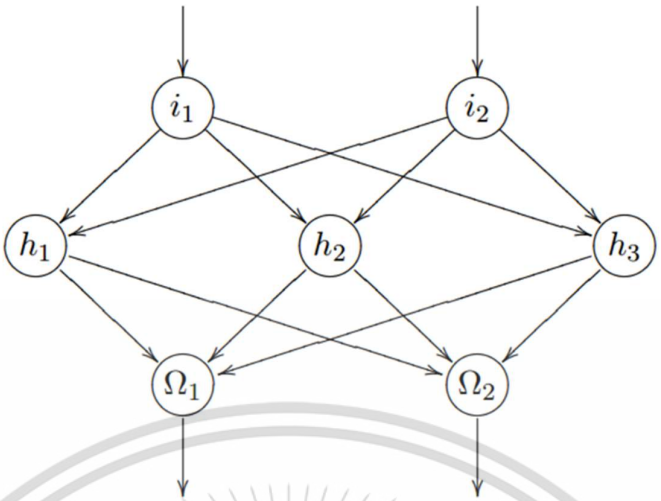

Figure 3.7 A feedforward network with three layers [40].

A brief introduction of backpropagation algorithm, the input unit first receives an input signal in a forward pass and the signal is continuously propagated to each hidden unit until reached the output unit. The received inputs are mathematically processed by the activation function at each hidden layer and forwards its calculated signals to the output unit. Each calculated signal is normally computed through an activation function at the output unit which forms response the network model. At this stage, the computed signals are generated from the activate function is comparatively analyzed with the target or desired output for finding the error of NN model. The final errors are found at the output unit and it is distributed back to the previous units and this process is repeated until the error goal is achieved or satisfied, hence, these feedbacked errors are applied to adjust the weights for all units of NN until a minimum error is achieved or converged and the result is satisfied [35].

3.3.2 Radial basis function network (RBFN)

RBFN has been traditionally associated with radial functions in a single layer network as shown in Figure 3.5. Radial function is simply a class of functions; they can be employed in any sort of model for linear or nonlinear and any sort of network for single layer or multi-layers. All n components of the input vector x feed forward to m basic functions, and the outputs are linearly combined with weights $\{w_j\}_{j=1}^{m}$ into the network output $f(x)$ [41].

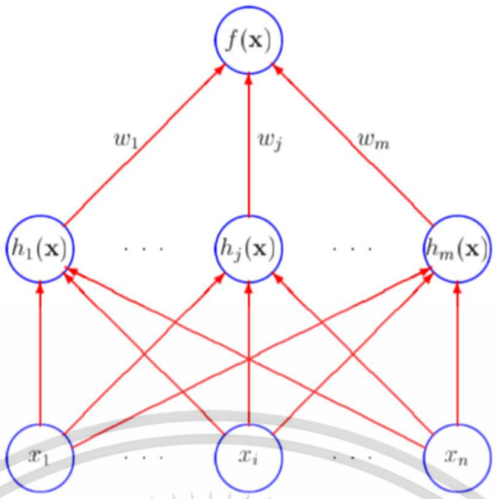

Figure 3.8 The radial basis function network [41].

3.3.3 Convolutional neural networks (CNN)

Convolutional neural networks are designed to process data, which is in the form of multiple arrays, for instance, a color image consists of three 2D arrays containing pixel intensities in the three-color channels. The key ideas behind convolutional NNs which take advantage of the properties of natural signals: local connections, shared weights, pooling and the use of many layers. The architecture of a typical convolution NN is structured as a series of stages. The first stage is composed of two types of layers: convolutional layers and pooling layers. The result of this local summed weights is passed through a non-linearity such as a rectified linear unit (ReLU). The role of the convolutional layer is to detect local conjunction of features from the previous layer and the role of the pooling layer is to merge semantically the similar features into one [42]. The inside of a convolutional network is performed in Figure 3.9, the figure shows each rectangular image of a dog is a feature map corresponding to the output for a part of learned features and its features are detected at each image position. The lower level features acting as oriented edge detectors, and a score is calculated for each image class in output as information flows bottom up.

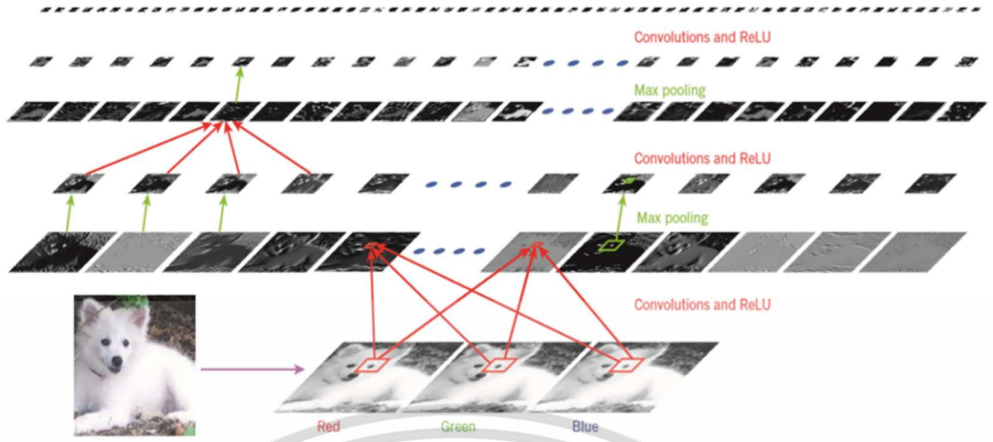

Figure 3.9 Interior of a convolutional network [42].

3.3.4 Recurrent neural network (RNN)

The input sequence one element is processed at a time for RNNs and maintaining in their hidden units a state vector which implicitly contains information about the history of all the past elements of the sequence [42]. When backpropagation is first introduced, it is applied for training RNNs. The tasks involve the sequential inputs such as speech and language. RNNs are very good at predicting the next character in the text [43].

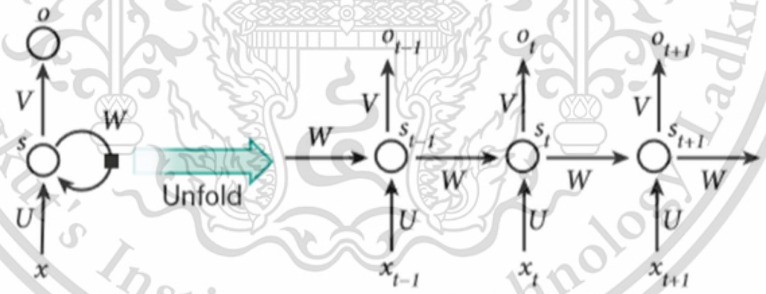

Figure 3.10 A recurrent neural network and the unfolding in time of the computation involved in forward calculation [42].

In Figure 3.5, the grouped hidden units of artificial neurons under nodes s with values s_t at time t obtain the input signals from other neurons at previous time steps that are represented with the black square, representing a delay of one-time step. Thus, RNN can map an input sequence with elements x_t into and output sequence with elements o_t, which o_t depends on all the previous $x_t^{'}$ ($t^{'} \leq t$). The same parameters (matrices U, V, W) are forwarded at each time step [42].

3.4 Initialization of neural network

3.4.1 Data preparation

The amount of dataset is firstly considered for creating the spread-F NN model. Hence, the initialization is to prepare the datasets for training the network model and test the network model. The datasets are divided into two parts for training and testing model. The training set is applied to train the predictor or classifier model and the testing set is parallelly used to validate the learning performance of NN model while training. On the other hand, the unknown dataset is already reserved for predicting, this reserved dataset is never applied in training before. Furthermore, the training datasets are stored by the matrix and divided into 70% for training and 30%. The given dataset covers three years from 2013 to 2015 for training and the unknown dataset is given by 2016 which will be used as a future data for predicting the future results.

3.4.2 Neural network procedure in implementation

1. Initialization, all the weights and threshold levels of the network are set as a random value and the learning rate is also given as α in a specific range ($0 < \alpha \leq 1$).

2. The back-propagation NN is activated by applying inputs $x_1(p), x_2(p), \dots, x_n(p)$ and desired outputs $y_{d,1}(p), y_{d,2}(p), \dots, y_{d,n}(p)$.

(a). Calculate the actual outputs of the neurons in the hidden layer:

$$Y_j(p) = f\left(\sum_{i=1}^{n} x_i(p) \cdot w_{ij}(p) - \theta_j\right), \tag{3.2}$$

where n is the number of inputs of neuron j in the hidden layer, and f is the sigmoid activation function.

(b). Calculate the actual outputs of the neurons in the output layer:

$$Y_k(p) = f\left(\sum_{j=1}^{m} x_{jk}(p) \cdot w_{jk}(p) - \theta_k\right), \tag{3.3}$$

where m is the number of inputs of neurons k in the output layer.

3. Weight training, the weights in the back-propagation network are propagated backward to each unit respectively for updating the weight values.

(a). Calculate the error gradient for the neurons in the output layer:

$$\delta_k(p) = Y_k(p) \cdot [1 - Y_k(p)] \cdot e_k(p), \quad (3.4)$$

where

$$e_k(p) = Y_{d,k}(p) - Y_k(p), \quad (3.5)$$

Calculate the weight correlations:

$$\Delta w_{jk}(p) = \alpha \cdot Y_j(p) \cdot \delta_k(p), \quad (3.6)$$

Calculate the weights at the output neurons:

$$w_{jk}(p+1) = w_{jk}(p) + \Delta w_{jk}(p), \quad (3.7)$$

(b). Calculate the error gradient for the neurons in the hidden layer:

$$\delta_j(p) = Y_j(p) \cdot \left[1 - Y_j(p)\right] \cdot \sum_{k=1}^{l} \delta_k(p) \cdot w_{jk}(p), \quad (3.8)$$

Calculate the weight corrections:

$$\Delta w_{ij}(p) = \alpha \cdot x_j(p) \cdot \delta_j(p), \quad (3.8)$$

Update the weights at the hidden neurons:

$$w_{ij}(p+1) = w_{ij}(p) + \Delta w_{ij}(p). \quad (3.9)$$

4. Iterations, increase iteration *p* by 1, go back to step 2 and repeat the process until the selected error criterion is satisfied or converged.

3.5.3 The test of neural network

The test of NN model is very important point which can be found after the end of training. The performance of the trained NN model can be evaluated by the error of the network model, generally, this performance of network model is derived from the error between the actual output and the predicted output which is performed by root mean square error (RMSE). Thus, this is an indicator of NN model which expresses the predictive accuracy of NN model. Eventually, the trained NN model provides a minimum RMSE is determined as the main NN model which is next applied in prediction.

3.5 The neural network performance and the implementation of neural network

3.5.1 The neural network performance

The performance of network model is previously mentioned and can be assessed by the error rate of outputs between the actual output and the desired output. The root mean square error (RMSE) has been popularly used to evaluate and determine the network model and other calculations. Also, this research applied the RMSE in determination of the NN parameters such as the number of hidden layer and neuron, and all input space parameters as shown in the equation 3.10. The selection of all parameters is based on the minimum RMSE which derived after training of the network model. That means which parameters provided the minimum RMSE is chosen and allocated as the main parameters of network model. Particularly, the RMSE has been successfully used in many researches [44], and [39].

$$RMSE = \sqrt{\frac{1}{N}\sum_{i=1}^{N}\left(Y_{pred} - Y_{obser}\right)^2} \tag{3.10}$$

where N is the number of data points, Y_{pred} represents the predicted data from NN and Y_{obser} represents the observed data which is obtained from measurement or observation. This method is also achieved by [45].

3.5.2 Implementation of neural networks in MATLAB

Recently, the implementation of NN model are simply implemented by several programming languages. Hence, a choice of NN goes to MATLAB programming that all developed NN tools can be simply utilized. Nevertheless, there are some basic codes of NN can be directly generated by the tool box in MATLAB. For example, the below MATLAB programming codes are generated from the NN tool box in MATLAB.

```
% Load dataset

    Input = load('Location of your input file');

    Target = load('Location of your target file');

    Unknown = load('Location of your unknow file');

% Data division

    net.divideFcn = 'dividerand';
```

```
net.divideParam.trainRatio = '70/100';
net.divideParam.testRatio = '30/100';
net.divideParam.valRatio = '';
% Create the neural network and determining the hidden layers and number of nodes
Net = patternnet([30 30 30]);
% Define a training ratio
net.trainParam.epochs = 80;
net.trainParam.goal = 1e-3;
net.trainParam.lr = 0.003;
net.trainParam.show = 25;
% Set the network performance and training function
net.performFcn = 'mse';
net.trainFcn = 'trainlm';
% ConFigure the transfer function
net.layers{1}.transferFcn = 'logsig';
net.layers{2}.transferFcn = 'logsig';
net.layers{3}.transferFcn = 'logsig';
% Training the neural network
yTrain = train(net, Input, Target);
% Test the trained model with the unknown dataset
yTest = net(Unknown inputs);
% Display the network performance
Performance = perform(net, Target, yTrain);
```

The above MATLAB code is a fundamental code that can be generated by a tool box in MATLAB. Therefore, when it is applied in real implementation, there are

some sections need to be adjusted as the appropriateness and requirement in the real application. Because the generated code is always provided or generated as a default function.

3.6 Summary

An introduction to the background of ANN has been presented in this chapter including learning method and the types of NN. The implementation of NN with MATLAB tool is also briefly described as step by step and some basic NN codes are presented. For more details, the information of NN can be seen in the references in this chapter.

CHAPTER 4
SPREAD-F NEURAL NETWORK MODEL FOR CHUMPHON STATION

4.1 Introduction

This chapter presents the spread-F neural network model consisting the significant parts of creation of spread-F neural network model. The initial determination of network structure is also explained and how to find the optimal input parameters are described with the experimental results.

4.2 The ionospheric data

The use of ionospheric data in this thesis is mainly obtained from Chumphon (CPN) station. This observation station has been installed in CPN since 2005 under the SEALION project for monitoring and predicting the disturbance in ionospheric layer over CPN area [46]. The ionospheric data so called ionogram data which is obtained by the observation of FMCW ionosonde. The ionogram data can be obtained in time intervals such as 1 minutes, 2 minutes, 5 minutes, 15 minutes, 30 minutes and 1 hour, respectively. Consequently, the ionospheric parameters can be gained by using scaler software which is called a special software. This software is particularly created and developed for this research. As shown in Figure 4.1, the ionogram data is in figure format showing the more details of ionospheric data.

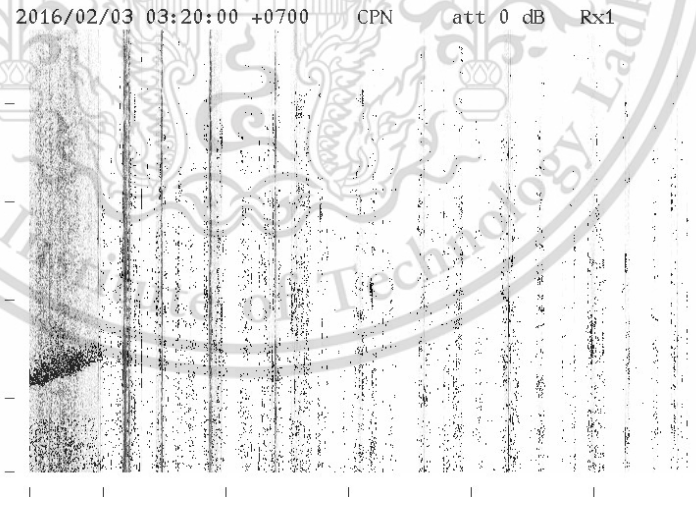

Figure 4.1 The ionogram data from FM/CM ionosonde.

This ionogram data is manually scaled using Special Software (special-10C-2000-eng) for each ionospheric parameter. The spread-F value is scaled and marked by binary number as the conditions of spread-F event depended on the types of spread-F

including frequency spread-F (FSF), range spread-F (RSF), mixed spread-F (MSF) and strong spread-F (SSF). The spread-F values are arranged in the file format as shown in the Figure 4.1 based on day and local time. Each letter represents the type of spread-F such as the range spread-F is marked by 'R', 'E' is of frequency spread-F and strong spread-F is represented by 'S'. In terms of blank spaces or without letter mean that there is no the occurrence of spread-F event at that time. The missing or damaged data is excluded reasoning it cannot be scaled, therefore, if there are some missing spread-F datasets can be noticed by the next section of the availability of dataset. In additions, the spread-F value is sampled at fifteen-minute interval from 18:00LT to 06:45LT as the periodic occurrence of spread-F event. Such the spread-F event is considered by two states of its occurrence, namely, spread-F presence is then represented by '1' and spread-F absence is specified as '0'. The scaled spread-F is gained in a text file format which is arranged a math file corresponding to year, day, and local time.

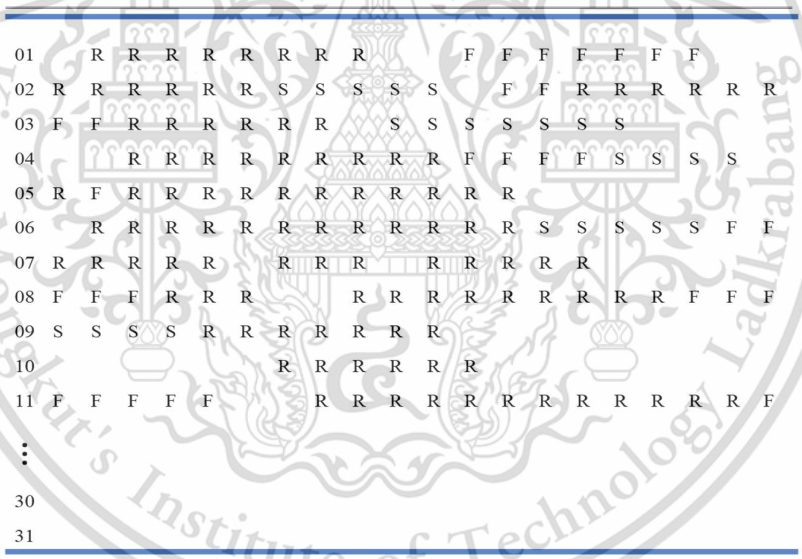

Figure 4.2 Spread-F data format.

4.2.1 The availability of dataset

The datasets are acquired from 2013 to 2015 during moderate period which are only used for training the NN model. As shown in Figure 4.2, there are some missing datasets caused by the downtime and damaged data file. Then the remaining available datasets are applied without any estimations for the missing datasets. As shown in below figures, the availability of data is percent expressed for all chosen years. The missing data is observed in January, February, March, April and May in 2013. These

datasets are then excluded from our NN model. During the middle of 2014, some missing datasets are observed as well.

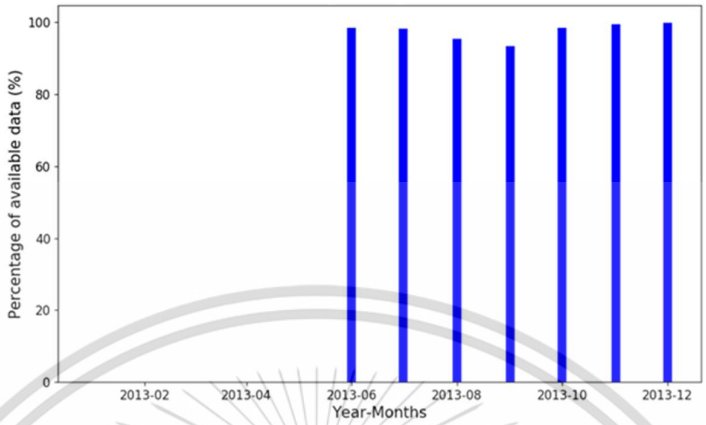

Figure 4.3 Availability of ionogram data in 2013.

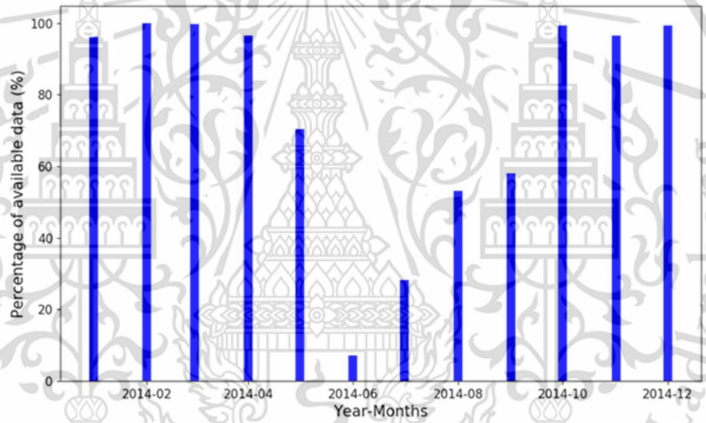

Figure 4.4 Availability of ionogram data in 2014.

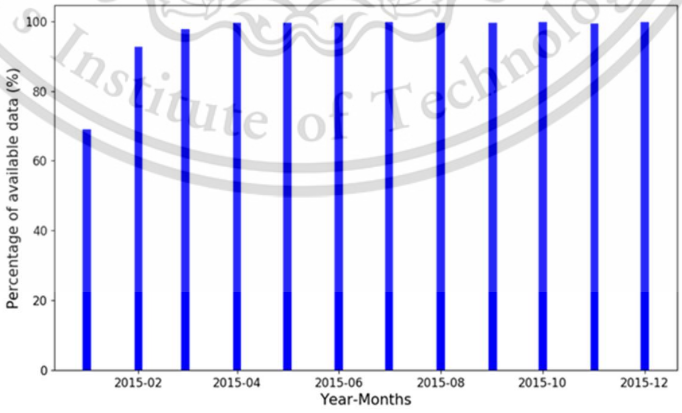

Figure 4.5 An availability of ionogram data in 2015.

The above graphs show the amount of the percentage availability of ionogram data. The training dataset covers three years from 2013 to 2015; this dataset is randomly

divided into 70% and 30% for training NN model. The dataset in 2016 is determined as the unknown or unseen dataset that is represented the future dataset which NN model is not aware of this data before. As shown in Figure 4.6, the amount of available dataset is available approximately 85% from January to September. On the contrary, the missing datasets are lost by about 10% to 35% from October to December as shown in Figure 4.6. In the case of missing data, they are not estimated or interpolated in any way.

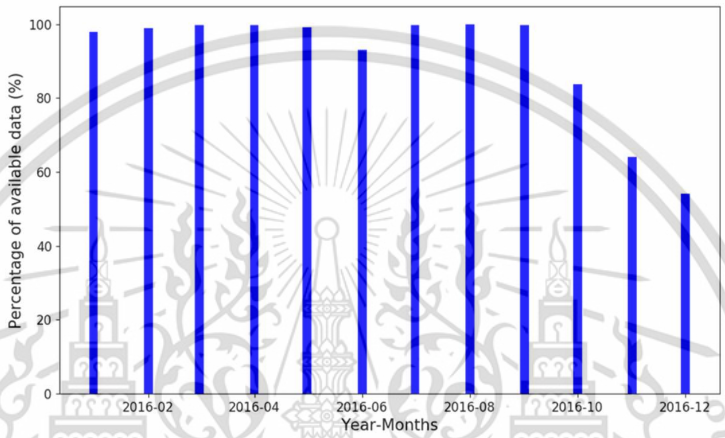

Figure 4.6 An availability of ionogram data in 2016.

4.2.2 Chumphon spread-F neural network model (CSNN)

CSNN model is improved by studying the weak points and the advantages of the previous NN model that has been completely done. For example, the prediction model of foF2 has been proposed by [6, 47]. The prediction of spread-F event is first proposed in Brazil by [12]. The application of NN model is proposed as a developed model for predicting the probability of spread-F occurrence over Brazilian sectors [5]. The International Reference Ionosphere (IRI-2012) model is a global model that globally provides the statistics of spread-F for many regions around the world [4]. However, the produced results from IRI model are not always close to the true measured results of real observations. Thus, this thesis attempts to study the spread-F statistics and improving the NN model for predicting spread-F occurrences at CPN station.

4.2.3 The input spaces

The correlations between the input parameters and desired outputs or targets are very dominant for creating the spread-F model. Therefore, the spread-F events are referred and investigated by various researches, the behavior of spread-F events

occurred and varied as the variability of solar activities, the magnetic activity, seasonal variations, diurnal variations, etc. Correspondingly, the uplift of F layer height [25], the F2 peak height, vertical plasma drift, and gravity waves are believed to affect the development of spread-F process as well. However, selection of input spaces is considerably achieved with six space inputs that associate the occurrence of spread-F events, which compose of F10.7 index, which is the excellent indicator of solar activity, Ap index represents the Earth's magnetic activity, seasonal variations (DNS and DNC) and diurnal variations (HrS and HrC) as already described in chapter 2.

4.3 The investigation of an optimum neural network architecture

The determination of NN model is major important for gaining the good model and there are several approaches has been completely proposed. Hence, we concerned the architecture of NN model evaluating the accuracy which is denoted by RMSE of NN model after training. The all original input spaces are initially used to determine the architecture of NN model without any average of them. The NN architecture is variously adjusted in many types as designed model including the number of hidden layer and neuron. After training of NN model, the RMSE is the indictor for selecting the NN model as shown in Figure 4.7. That results are obtained from training with various number of hidden layers and neurons. Therefore, which NN model produced the minimum RMSE, it is determined to be the main NN model for examining the input spaces.

4.3.1 Single hidden layer

An initial determination of the hidden layer begins with single hidden layer containing 10 nodes. For each training of single hidden layer, the number of neurons is orderly increased by 5 nodes per time from 10 to 60 neurons and there is only one network model which is chosen by examining the RMSE among them. The best performance of NN model is minimum RMSE at 0.2431 corresponding to 45 neurons of single hidden layer as illustrated Figure 4.7. Then if this NN type is used it should be concerned on this result.

4.3.2 Two hidden layers

Determination of the NN architecture is continued by increasing the number of hidden layers. The hidden layer is enhanced from a single layer becomes two hidden layers that contains the different number of neurons from 10 to 60 neurons. The NN

model is trained like the implementation of single hidden layer as above section. For each training, its results indicate the difference of NN model's performance as shown in Figure 4.7, the best performance of two hidden layers is found by 0.1902 at 50 neurons for two hidden layers. These 50 neurons of two hidden layers are then the best NN model in this case.

4.3.3 Three hidden layers

The experiment is repeatedly operated by increasing the number of hidden layers to three hidden layers. In this section, the three hidden layers is implemented like the single and two hidden layers as previous two sections. The minimum RMSE are noticed as a lowest RMSE which appeared at 0.1854 corresponding to 45 nodes as shown in Figure 4.7. As we have determined three different hidden layers and various number of neurons, we finally detected the best performance of NN model in these three hidden layers containing 45 neurons in each hidden layer as the proposed NN model in this thesis.

According to the results of each experiment, the amount of experiment results is comparatively analyzed and the selected NN model consists of three hidden layers and each hidden layer contains 45 nodes are provided the best performance of NN model with minimum error as shown in Figure 4.7. Then, this NN architecture becomes a main NN model for predicting spread-F events at CPN station.

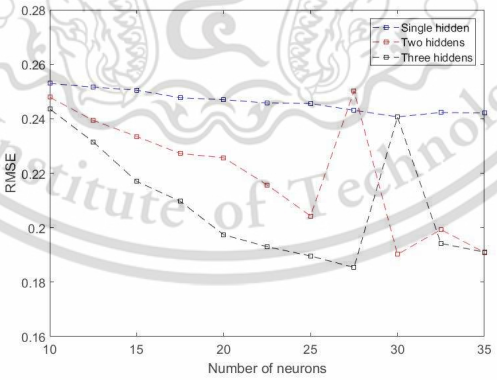

Figure 4.7 Comparison of the performances of three types of hidden layers and nodes.

4.4 The investigation of optimum input parameters

The optimum input parameters are an important part of NN model after the NN architecture is already selected. For this reason, the input parameters are certainly

considered for both F10.7 radio flux and Ap index. The determination method of these two input parameters are derived from the average of previous values as a given interval. All inputs are initially scaled into a specific range between 0 and 1 before they are utilized into the NN model for training.

4.4.1 Seasonal variations

The seasonal variations correspond to spread-F events that can be referred as observing in the historic statistics of spread-F occurrence [26]. The cycle of season variations is commonly divided into four main seasons which respond to the Earth's rotation around the sun, hence, the characteristic of spread-F events differently occurs in each season. The occurrence of spread-F event is an instability change which can be studied by analyzing the ionospheric parameters such as F10.7 index, h'F, hmF2 and Ap index. However, seasonal variations become a factor that is applied in this NN model representing the spread-F event of each. The variability of season is generated by day number which is converted by cyclic component as

$$DNS = \sin\left(\frac{2\pi \times DN}{365}\right), \tag{4.1}$$

and

$$DNC = \cos\left(\frac{2\pi \times DN}{365}\right), \tag{4.2}$$

where DN is the day number, $0 \le DN \le 365$.

4.4.2 Diurnal variations

According to the spread-F occurrences are corresponded to time variations. The spread-F variations in a day is hourly observed during night time from 18:00LT to 06:45LT. Thus, the diurnal variations are indicatable to the development of spread-F event. This relationship between diurnal variations and spread-F events, the diurnal variation is importantly included in many ionospheric models. Variability of time is represented by functions of hour number which is computed in cyclic component for generating the cycle of time changes as,

$$HrS = \sin\left(\frac{2\pi \times HR}{24}\right), \tag{4.3}$$

and

$$HrC = \cos\left(\frac{2\pi \times HR}{24}\right), \tag{4.4}$$

where Hr is the universal time, it is represented by an integer in the range of $0 \le HR \le 23$

4.4.3 Determination of F10.7 radio flux

The widely used proxies of solar activity are the sun spot number (SSN) and F10.7 radio flux. In this case, F10.7 radio flux is utilized instead of SSN. We consider the average of previous hourly F10.7 index values, whereby F10.7 is hourly acquired from the data center [28]. We initially applied F10.7 index value beginning at original values and followed by the average of the previous values, respectively. The running mean values of F10.7 index is orderly listed consisting of a original value represents F10.7 index values which are not averaged, 15days (15d) for the average of the previous 15 days of F10.7 index values, 1 month is represented by 1m for the previous 30 values, 2m for the previous 60 days, 3m represents the previous 3 months, 4m is of the previous 4 months, 8m and 12m, respectively. The horizontal axis represents the given steps of F10.7 index and the vertical axis represents the RMSE.

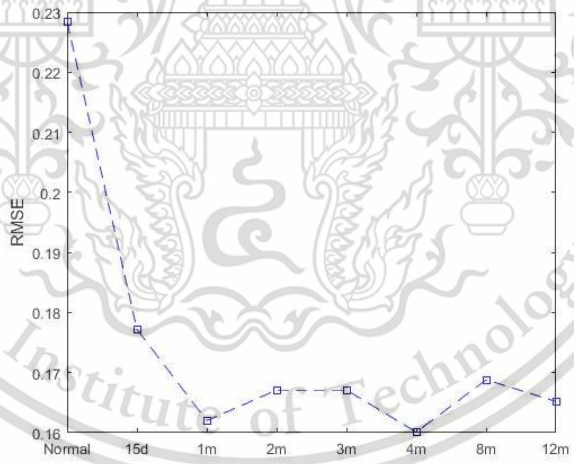

Figure 4.8 RMSE of each average of F10.7 index.

The optimum F10.7 values based on the minimum RMSE as illustrated on the graphs. The running mean values of F10.7 is respectively trained with the optimum NN architecture to find the optimum F10.7. As a result, the optimum F10.7 values are found at the average of the previous 4 months of F10.7 index values. The minimum of RMSE is 0.1601 as illustrated in Figure 4.8. Therefore, this average of the previous 4 months

of F10.7 index value (F10.7(4)) is chosen to be a part of input spaces for this spread-F model.

4.4.2 Determination of magnetic activity

The Ap index represents the variability of the Earth's magnetic field which indicatable the irregularity of magnetic field which may be a cause of the occurrence of spread-F event in some case. Thus, Ap index has been used to describe several phenomena in the ionospheric and storm events due to variability of magnetic equator field. Ap index is a global average value from 13 magnetometers around the world, Ap index values are provided at every 3 hours from data center [28]. Then Ap index is designed as the original value, 4 represents the average of the previous four 3hourly of Ap index values, 8 is of the average of the previous eight 3hourly of Ap index values, 16, and 32, respectively. The investigation of Ap index is respectively calculated as the running mean values, each designed Ap index is trained with the optimum architecture of NNs. The Ap averaged index is represented by horizontal axis and RMSE is along vertical axis.

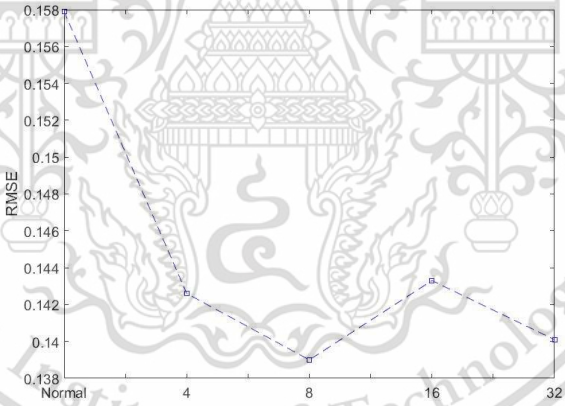

Figure 4.9 RMSE of each average of the previous value 3hourly of Ap index values.

As the result, the NN model are trained with several averages of Ap index for finding the Ap index which provides the minimum error. Then, the Ap index provided the minimum RMSE corresponding to the average of the previous eight 3-hourly Ap index values as illustrated in Figure 4.9. Therefore, Ap(8) is defined as an optimum input space for our model and it is applied as a main input parameter with another inputs for training the model.

4.5 Chumphon spread-F neural network model (CSNN)

The achievement of determination of each parameter provided the best performance of NN model as shown in the previous sections. The creation of spread-F NN model is completed by combining all investigated parameters together. As results, the NN model is obtained by combining the optimum architecture and the optimum input spaces are shown in Figure 4.17. The NN model consists of six input parameters and three hidden layers which contain 30 neurons in each hidden layer. The spread-F NN model corresponds to the two characteristics of spread-F including spread-F presence and spread-F absence.

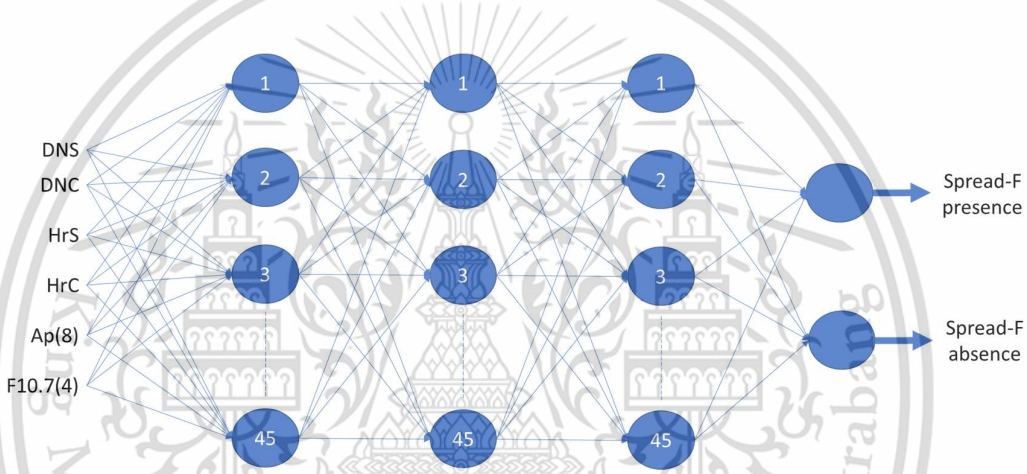

Figure 4.10 Chumphon Spread-F Neural Network Model.

4.6 The training property of spread-F NN model

After training, the properties of NN model are described in a confusion matrix as shown in Figure 4.11. The target class is divided into two classes as the attributes of spread-F events, namely, spread-F presence is defined for target class 1 and target class 2 is assigned for spread-F absence. Similarly, the output class must to rely on the target class which is composed of two classes as well. All the spread-F samples are applied for training the NN model consisting of 78,114 samples from 2013 to 2015.

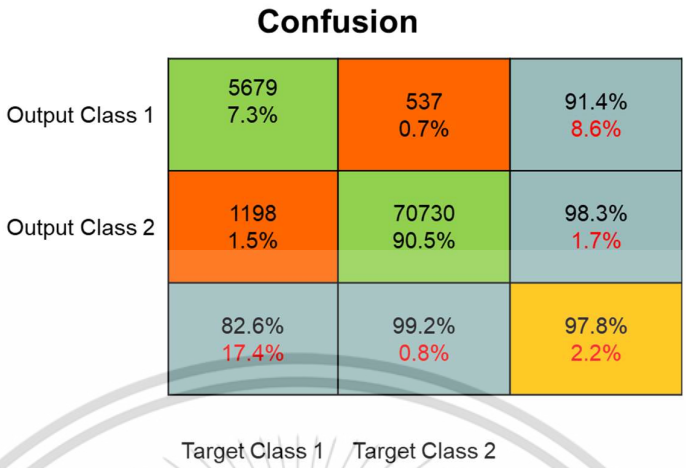

Figure 4.11 The performance of the NN spread-F model after training.

The first two diagonal cells show the number and percentage of correct classifications by the trained network. For example, 5,679 occurrences are correctly classified as spread-F presence. This corresponds to 7.3% of all 78,114 data samples. Similarly, 70,730 cases are correctly classified as spread-F absence. This corresponds to 90.5% of all data samples.

The amount of 537 cases of the spread-F presence is incorrectly classified as spread-F absence corresponding to 0.7% of all 78,114 samples in the data. Similarly, 1,198 of the spread-F absences are incorrectly classified as spread-F presence corresponding to 1.5% of all data.

Out of 6,216 spread-F presence predictions, 91.4% is correct but 8.6% is wrong. Out of 71,928 spread-F absence predictions, 98.3% is correct and 1.7% is wrong. Out of 6,877 spread-F presence cases, 82.6% is correctly predicted as spread-F presence and 17.4% is predicted as spread-F absence. Out of 71,267 of spread-F absence cases, 99.2% is correctly classified as spread-F absence and 0.8% is classified as spread-F presence. Overall, 97.8% of the predictions are correct and 2.1% is wrong classifications.

4.7 Summary

The optimum architecture of NN model and suitable set of input parameters are achieved by selecting the best performance from the experiment results. The optimum spread-F model consists of six main input parameters including seasonal variations

(DNS and DNC), diurnal variations (HrS and HrC), Ap(8) and F10.7(4). The number of hidden layers provided the best performance including three hidden layers with 45 neurons in each hidden layer. This optimum spread-F model is called CPN Spread-F Neural Network model (CSNN) and this is a developed model for predicting the spread-F event at CPN station.

CHAPTER 5
RESULTS AND DISCUSSIONS

5.1 Introduction

This chapter totally presents the experimental results that acquired from both the observations and predictions. The accuracy of NN model is visualized by considering in a part of comparative analysis. Similarly, the NN model performance can be evaluated in term of error analysis in the last section as presented.

5.2 Characteristics of ESF in CPN station

5.2.1 Observations of spread-F occurrence

The occurrence of spread-F events is different in each day, month, year, location (latitudes and longitudes) and solar activity. There are many related factors that affect the occurrence of spread-F events. For instance, seasonal variations, diurnal variations, solar activity, uplift height of F layer, and magnetic activity as previously mentioned. These factors are mentioned and have been utilized as the input parameters for spread-F model in Brazil. The observed spread-F is analyzed by the percentage of spread-F occurrence for monthly and yearly basis. Therefore, the predicted spread-F is popularly demonstrated in a percentage of spread-F occurrence as presented in the results. The percentage of spread-F occurrence can be computed from

$$Spf_{prob} = \frac{\sum Spf_{occur}}{T_{obs}} \times 100 \qquad (5.1)$$

where Spf_{prob} is the probability of spread-F occurrence, Spf_{occur} represents the occurrence of spread-F that is obtained from the observations, and T_{obs} is the total number of the observed spread-F.

5.2.1 Statistics of spread-F occurrence

The spread-F events have been studied by many researchers. Particularly, in low latitude region nearby the magnetic equator which is played the important role for the ionospheric irregularities. The various published researches indicate that the equatorial spread-F event occurred more often in low latitudes and the ionospheric layer is also more disturbed by the instability of ionosphere in this region. Therefore, this research aims to study the equatorial spread-F by analyzing the spread-F data which is observed at CPN station near the magnetic equator. CPN station is in the Southern of Thailand as shown in Figure 5.1.

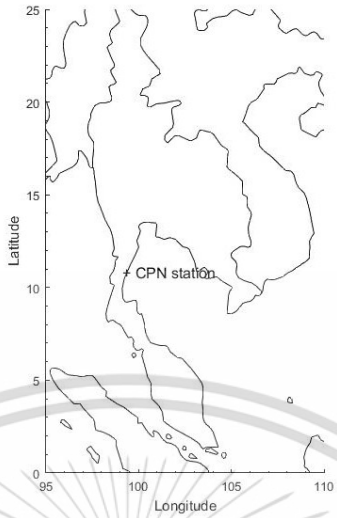

Figure 5.1 Geographic location of CPN station in Thailand.

The range spread-F (RSF) was manual scaled between 18:00 LT and 06:45LT as the appearance time of spread-F event as shown in Figure 5.2-5.3, that is the statistics of RSF occurrence in CPN station from 2013 to 2016. The statistics of RSF occurrence is plotted as the local time and months. The vertical axis shown respectively as the local time that starts at 18:00LT until in the morning 06:45LT and the horizontal axis represents each month scale depending on the availability of spread-F data. In Figure 5.2 (a) shows the statistical analysis of RSF occurrence in 2013. Note that January, February and November are not be shown in the graph caused by the disappearance of spread-F data. The RSF event frequently appeared in time intervals 18:00LT to 03:00LT for each month in 2013. The strong occurrence of RSF event is more seen in September and October as illustrated in Figure 5.2 (a). In 2014, the RSF event is observed and shown in Figure 5.2 (b), the inequality of graph scale along monthly axis is affected from the missing data. There are no spread-F data files in June and July, thus, they are excluded. The occurrence of RSF event mostly occurs after 18:00LT and disappears before 05:00LT. The total occurrence of RSF event is higher in the equinoctial months. Especially, the maximum occurrence of RSF event is observed in March and April for 2014 during moderate solar activity. In 2015, this year is a period of high solar activity of solar cycle 24. The observed RSF occurrence indicates that the maximum occurrence still appeared in March equinox more often than solstice months, excepted for 2013.

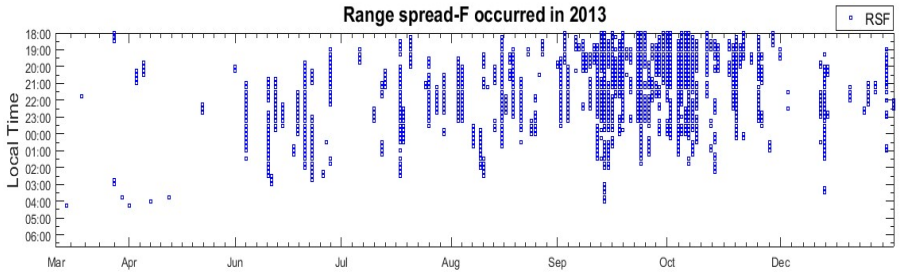

(a)

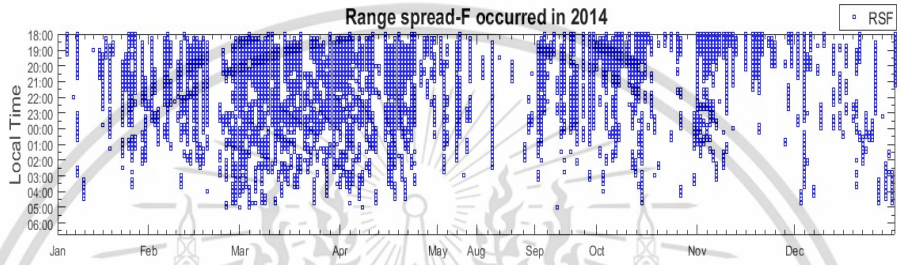

(b)

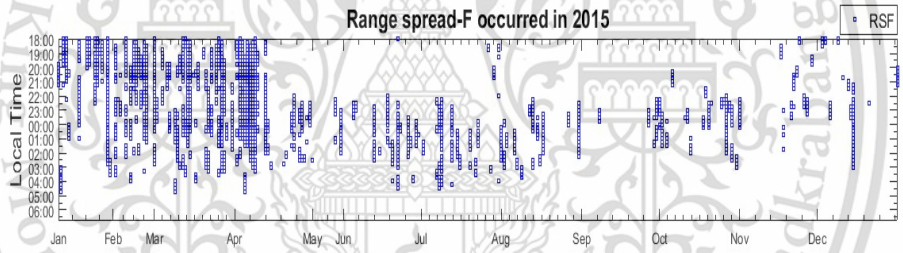

(c)

Figure 5.2 The RSF statistics from observation at CPN station from 2013 to 2015 is assigned for training the NN model.

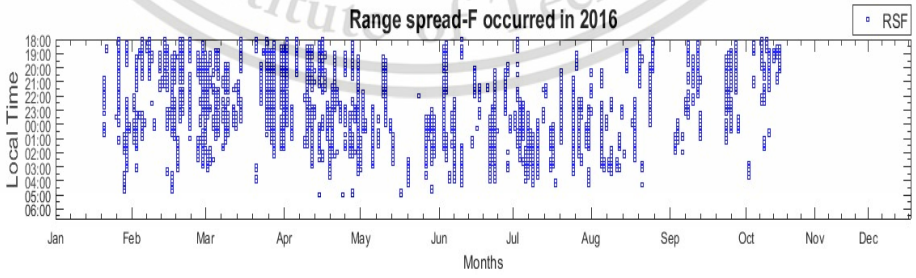

Figure 5.3 The RSF statistics are obtained from observation at CPN in 2016 for prediction.

The entire observed result illustrates the RSF event from 2013 to 2016 at CPN station. The above RSF statistics are applied to develop the NN model in training term of NN model. To validate the model, we supposed that the below RSF statistics to be future spread-F or unknown data that NN model have never seen before. These spread-F statistics will be applied to validate the trained NN model like prediction. Therefore, the NN model objective is to predict the occurrence of RSF event in 2016. However, the remaining issue in term of missing spread-F data file is seen in November and December in 2016 as shown in the Figure 5.3. The missing data is approximately guessed by the problems of ionosonde and during conversion of data file such as file damaged, file error, file lost and station down. As the observation results, RSF event is highly observed in equinoctial months than solstice months.

5.3 The results and discussion

5.3.1 The results of CSNN model

The CSNN model is trained with six input parameters including seasonal variations, diurnal variations, F10.7(4) index and Ap(8) index as presented. The results in this section are obtained by testing the CSNN model with an unknown dataset. The gained results indicate the prediction of NN model in 2016 and it is applied for validating the accuracy of CPNN model. Thus, the development of NN model is considered by analyzing these predicted results. The ability of trained NN model can be evaluated from the correlation between the observed and predicted results as presented.

The results of CSNN model are arranged as hour predicted in a day. The occurrence of spread-F event is shown in a percentage probability of spread-F occurrence as the vertical axis and the horizontal axis is a local time from 18:00LT to 06:45LT. As a result, the graphs show the comparison between the observed spread-F event as represented by the blue dot graph and the predicted spread-F from NN model is depicted by the red dot graph. Then the goal of these results is to show the ability of NN model in predictability of spread-F event at CPN station in 2016 respectively. As the activation function of NN model, the sigmoid function is used as the main function at each unit of NN model. Therefore, the produced results of NN model become the probability value as the sigmoid function. The two results of predicted and observed

values are computed with the threshold for deciding the probability of which result should be of spread-F presence or spread-F absence. We then use a soft decision to make the decision of the results by assessing the likelihood between both classes.

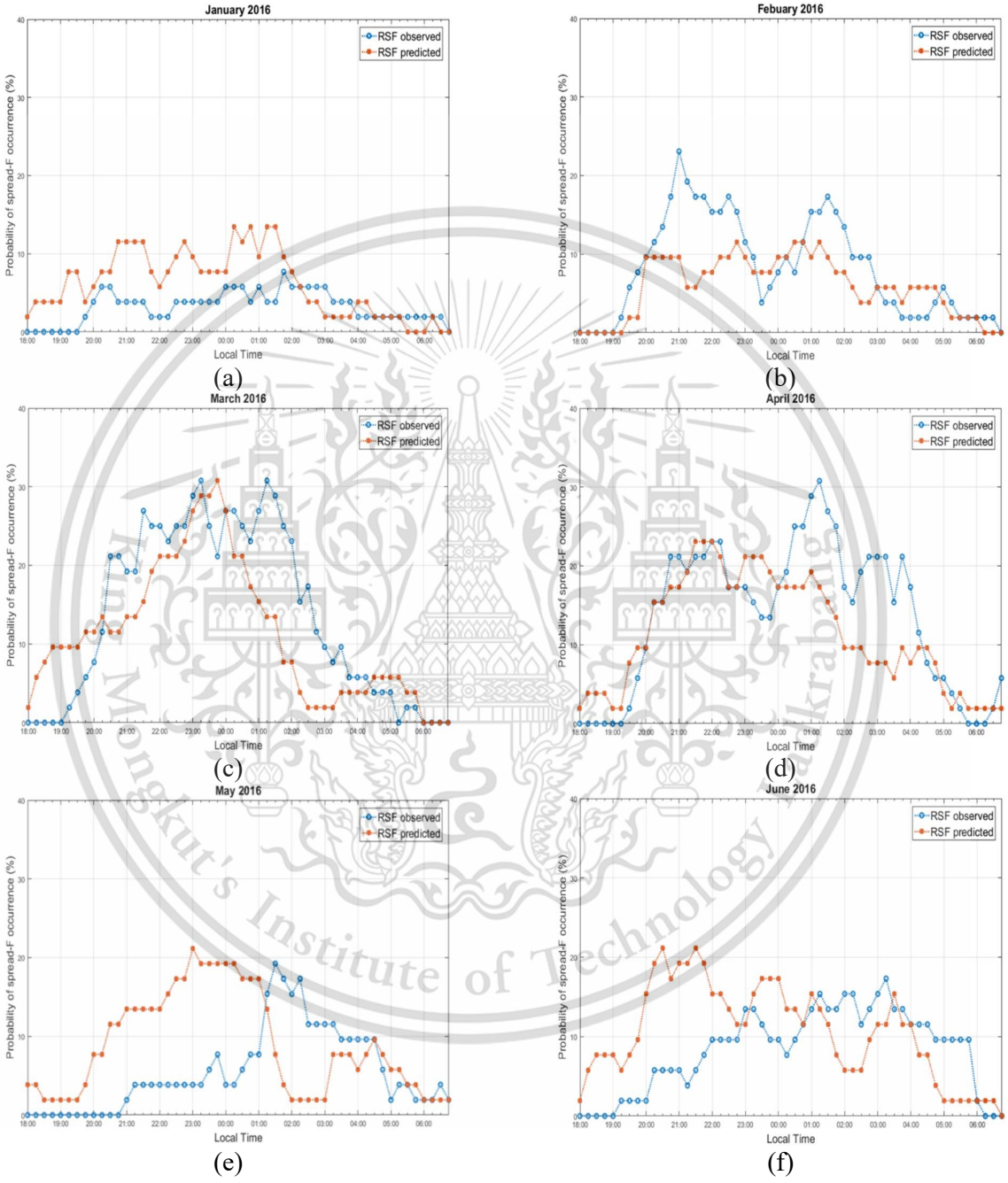

Figure 5.4 Comparison between the observed (blue dots) and predicted (red dots) probability of spread-F in 2016 at CPN station.

The results are respectively described for a first half of year as shown in Figures 5.4 (a) – (f), the results mainly show the comparisons between the predicted results and

the observed results in January to June in 2016. As the comparison results, the predicted results of NN model almost correlate with the real observed results, for example, we see that the NN model overestimates the percentage of RSF occurrence about 15% during18:00LT to 01:00 LT in January, May, and June, respectively. On the other hand, NN model also oppositely provides the underestimated RSF occurrence during 20:00LT and 04:00LT in February, March and April, respectively. Similarly, the same cases are noticed during 01:00LT to 05:00LT in January, May and June as demonstrated in Figure 5.3 (a), (e) and (f). As a result, the percentage probabilities of spread-F occurrence are dissimilar for all times, but the deviation of predicted results is still lower than 20% for both cases of predictions as illustrated in Figure 5.4 (a) – (f). Overall, we seen that the first four months (Jan, Feb, Mar, and Apr) are better in agreement than the last two months, especially, the obtained results are noticed that the predicted values of the proposed model which more closed to the observed values are seen in equinoctial months. Then, these first considered results can be indicated that the prediction of NN model is slightly better in agreement with the higher percentage occurrence of RSF event than lower percentage occurrence of RSF event as shown in each Figure 5.3, respectively. Consequently, more differences are clearly found in May and June along entire times in June solstice months. We then can conclude that the good agreement of NN model is most satisfied in March equinoxes and September equinoxes.

Secondly, we continuously analyze the second parts of results as shown in Figure 5.5 (a) – (f). These second results are aimed to present the same purpose as the above mentioned of the results of NN model and the observed results. As the results in July, the NN model provided the over prediction of RSF occurrence approximately 9% from 18:00LT to 00:30LT and the predicted values are lower than observed results by approximately 18% between 00:45LT and 05:00LT as shown in Figure 5.5 (a). The highest overestimation of NN model is observed in August in time intervals between 21:00LT to 23:45LT, the highest estimated percentage of RSF occurrence is approximately 26% as illustrated in Figure 5.5 (b). Moreover, the NN model underestimated the percentage of RSF event after midnight to 06:00LT in July and 03:30LT to 06:00LT in August. Accordingly, we notice that the overestimation of the proposed NN model produce the over values for all the times September and October as shown in Figure 5.5 (c) and (d). These overestimate values are approximately 18% and although the predicted results are exactly overestimated, but the trends of graph are

still similar or closer to the real observed results as demonstrated in Figures 5.5 (c) and (d). We notice that the low amount of ionogram data file in November and December than other months in 2016 as shown on the graph of the available data in Chapter 4. However, the missing data is already excluded from November and December, additionally, the scaled results are observed without RSF occurrence in these two months, even though the NN model similarly predicted the existent probabilities of spread-F occurrence in both months as demonstrated in Figures 5.5 (e) and (f). These overestimated results probably corresponded to the learning of NN model that is trained with the high spread-F occurrence during this period and why it produced the overestimation of the high probabilities of RSF occurrence. We also prove that those results are probably caused as the disappeared of data. The predicted RSF occurrence is lower than 16% in November and 19% of December. Eventually, although the predicted results are higher or lower than the observed result, they are still acceptable for the first version of NN model.

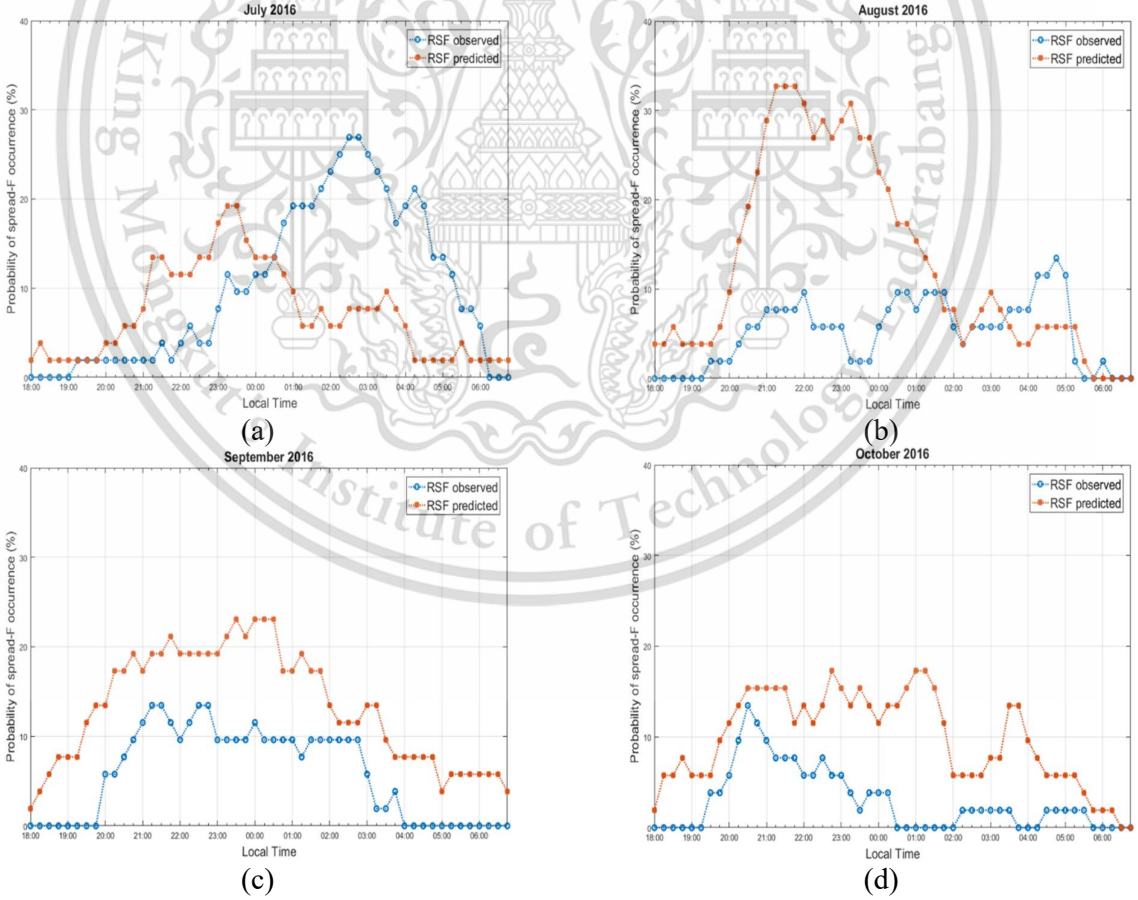

(a) (b)

(c) (d)

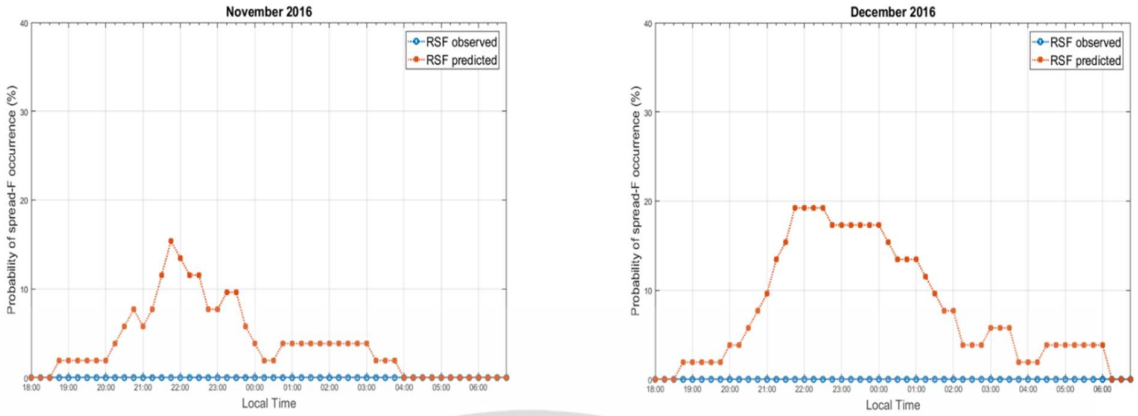

(e) (f)

Figure 5.5 Comparison between the observed (blue dots) and the predicted (red dots) probability of spread-F in 2016 at CPN station.

The resulting CSNN model is compared with the observed results to validate the performance of NN model. The observed results are indicatable that the percentage probabilities of spread-F occurrence are obtained from the measurement in CPN station. The predicted results are indicatable the attempts of this thesis try to develop the prediction model of spread-F events for CPN station using NN method. The derived results of spread-F NN model are mainly obtained from calculation techniques of NN algorithm, the results are statistically expressed in the percentage probabilities of spread-F occurrence based on long term statistics. The comparative analysis identifies the deviations of NN model which are compared with the real observed results, the feedback of the proposed NN model totally produced the highest overestimate results in July and August. On the other hand, the underestimations of NN model are observed in other months not more than 20%.

5.3.2 The deviation analysis of NN model

The accuracy of CSNN model is validated by evaluating the deviation values between the NN model result and the observed values. We then simply compute the deviation by subtracting between the predicted result and the observed result plugging them into percentage. As shown in Figure 5.5, the deviated results of NN model from real observation. The positive value indicates that the predicted results of NN model are higher than the observed results at that time, where the negative value represents that the underprediction of CSNN model which provides lower results than the observed results at the same time. The overall deviated results are satisfiable by the deviation probabilities low than 30% as shown in Figure 5.6.

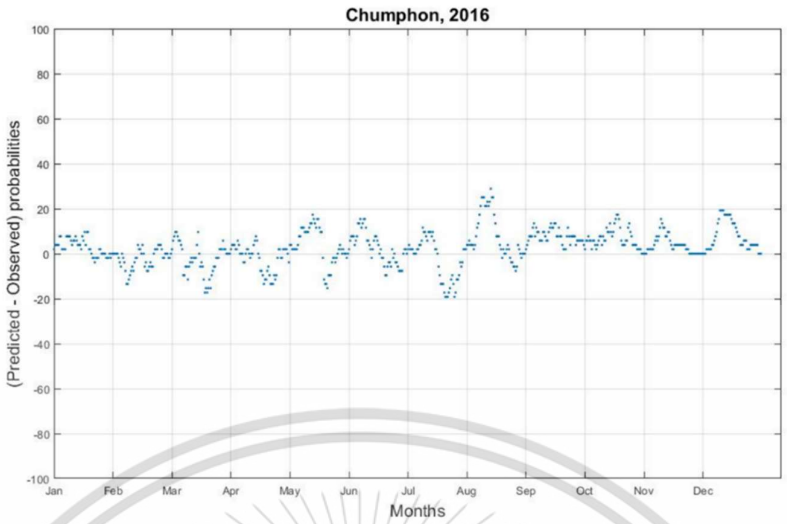

Figure 5.6 The deviation between the NN model prediction and the observation results.

5.4 Summary

The RSF occurrence good corresponded to time variations and seasonal variations evidently. The big picture of RSF occurrence cannot be confirmed for each year as the observed results. The proposed NN model can predict the occurrence of RSF event and the results of proposed NN model almost correlated with the observed results as presented. However, there are some uncover cases must be improved and the proposed NN model will be improved the prediction accuracy of CSNN model.

CHAPTER 6
CONCLUSIONS

This thesis is concluded in this section including summary of the obtained results and a further objective on spread-F predictions applying the technique of NNs. The development of NN spread-F model is the aim of this study for predicting the spread-F occurrence utilizing an ionosonde measurements from CPN region. The results indicate that NNs are suitable for spread-F predictions with the following input parameters: seasonal variations (DNS and DNC), diurnal variations (HrS and HrC), a 4-previous running mean of the daily F10.7 radio emission (F10.7(4)) and the running mean of eight 3-hourly magnetic Ap index values (Ap(8)).

6.1 Discussions

The spread-F occurrence has been studied in terms of the monthly percentage occurrence. The irregularity of ionospheric spread-F is clearly mentioned by Rayleigh-Taylor (R-T) instability mechanism. The generation of spread-F is responsible to the computing processes of linear growth rate for the R-T instability as the suggestion. The spread-F occurrence is well characterized by the diurnal, seasonal, solar activity and magnetic activity. Moreover, the rate of range spread-F occurrence higher occurs in CPN region near the magnetic equator.

According to the spread-F data format is utilized in this study, the spread-F occurrence is represented by a measure equal to one while the absence of spread-F is represented by zero. Because the outputs from NN provided a value in range between zero and one for both classes, which represents the presence and absence of spread-F events. Consequently, this provided spread-F is a likelihood of spread-F of two classes and this provided spread-F must be converted to a one and zero before calculating the monthly percentage of spread-F. For this research, the NN results are calculated and illustrated in the percentage probabilities of spread-F occurrence. The predicted spread-F and observed spread-F are compared for validating the performance of NN model. As the statistical analysis of RSF occurrence is observed, the range spread-F occurs in equinoctial months higher than solstice months for CPN region as presented.

This study will help in determining the actual spread-F onset conditions and it can be developed. The major drawback in spread-F forecasting is relied on amount of spread-F dataset. Thus, the amount of spread-F dataset must be increased for training

the network model, because the larger dataset can be distributed the probability of spread-F occurrence covers more situations of spread-F event. The case of input parameters, it is clearly seen in our experiments that when the number of input space are added to the network model, found that the accuracy of network model is also improved as the association of input with spread-F event, then the new inputs are considering for development of the network model, for example the uplift of F height layer, the peak height of F2 layer, vertical plasma drift, etc. In term of network architecture model, the obtained results indicate that each designed network model provided the different performances, then the optimum solution is determined by selecting the optimum results as presented. Thus, the applied technique is used to define all parameters as an optimum parameter is more useful to enhance the performance of NN model as shown in each experiment result.

The day-to-day variability of spread-F occurrence is caused by the origins of spread-F seeding perturbation source that initiates R-T instability [48]. The factors are believed to associate this day-to-day variability including gravity waves which has been cited as main causes of the day-to-day variability and the other factor is the equatorial ionization anomaly, which has been found to strengthen in the afternoon of spread-F days. However, this input parameters probably help to improve the NN model's performance for predicting the day-to-day variability of spread-F occurrence and some rapid variations during individual nights.

6.2 Summary

The following is a summary of the results of this study:

- A neural network with three hidden layers and thirty nodes for each hidden layer was found to be optimal for spread-F predictions.
- The seasonal (DNS and DNC), diurnal (HrS and HrC), magnetic activity (Ap(8), a running mean of the previous eight 3-hourly Ap index values) and F10.7 index (F10.7(4), a thirty-day running mean of the F10.7 values) were determined as optimum for spread-F forecasting.
- The accuracy of our proposed NN model is 97.8% for correct classification.
- A NN single station model was developed with range spread-F data from CPN. The predicted results were compared with observed results as presented and discussed.

- A comparative analysis of the CSNN model and the observation of spread-F in CPN has been shown that NNs can be used to predict the occurrence of spread-F.
- The deviation of proposed NN model is lower than 30% and a good agreement of this proposed NN model is the equinoctial months than solstice months.

Finally, as the following of succeeded studies of spread-F model has been presented. The equatorial spread-F events are an inconstant irregularity which more difficult to correctly predict its behaviors. Even though the completed spread-F model can provide a good result in a specific area, but it still come with some weak points of efficiency are quite low in some cases. Therefore, this is a condition which bring this study to CPN station for improving the prediction model of spread-F.

6.3 Future works

This study will be extended to the other locations near the geomagnetic equator and improved the NN model's performance. The new input parameters will be applied for development of the spread-F prediction model. Another important consideration will be the day-to-day variations of spread-F. Therefore, the factors that are believed to cause the daily variability including the F layer height, gravity waves, vertical plasma drift, equatorial ionization anomaly, thermosphere winds and F2 peak height. These will be examined in the input space for spread-F predictions in the attempt to model the daily variability.

In conclusion, this thesis has shown that NNs may be applied to develop a prediction tool for the spread-F occurrence, however, significant effort is required to improve the database available and refine the inputs known to influence spread-F occurrence.

REFERENCES

[1] F. W. Perkins, "Ionospheric irregularities," *Reviews of Geophysics,* pp. 1944-9208, 1975.

[2] N. Kenro, "FMCW Ionosonde for the SEALION Project," *The National Institute of Information and Communications Technology,* pp. 287-298, 2009.

[3] S. Saito and T. Maruyama, "Ionospheric height variations observed by ionosondes along magnetic meridian and plasma bubble onsets," *Annales Geophysicae,* pp. 2991-2996, 2006.

[4] IRI, "International Reference Ionosphere - IRI 2012: Virtual Ionosphere, Thermosphere, Mesosphere Observatory (VITMO)," 2012. [Online]. Available: https://omniweb.gsfc.nasa.gov/vitmo/iri2012_vitmo.html.

[5] L.A. McKinnell et al., "Predicting the probability of occurrence of spread-F over Brazil using neural networks," *Advances in Space Research,* pp. 1047-1054, 2010.

[6] N. Wichaipanich et al, "Prediction of foF2 using Neural Network at Thailand equatorial latitude station, Chumphon," *IEEE,* pp. 1-4, 2014.

[7] K. Watthanasangmechai et al, "TEC prediction with neural network for equatorial latitude station in Thailand," *Earth Planets Space,* pp. 473-483, 2012.

[8] O. Oyeyemi et al, "Near-real time foF2 predictions using Neural Networks," *Journal of Atmospheric and Solar-Terrestrial Physics,* pp. 1807-1818, 2006.

[9] Maitha H. et al, "Using MATLAB to Develop Artificial Neural Network Models for Predicting Global Solar Radiation in AI Ain City - UAE," *Engineering Education and Research Using MATLAB,* 2011.

[10] Berkner et al, "F-region ionosphere-investigations at low latitudes," *Journal of Geophysical Research,* vol. 39, no. 3, pp. 215-230, 1934.

[11] D. L. Helly et al, "Electrostatic plasma turbulence in the topside equatorial F region ionosphere," *J. Geophys. Res., 107(A10),* 2002.

[12] M.A Abdu et al, "Equatorial spread F statistics and empirical representation for IRI: A regional model for the Brazilian longitude sector," *Advances in Space Research,* p. 703 – 716, 2003.

[13] L. Rayleigh, "Investigation of the character of the equilibrium of an incompressible heavy fluid of variable density," *Proceedings of the London Mathematical Society,* vol. 14, p. 170–177, 1883.

[14] M.C. Kelley et al., The Earth's Ionospehere: plasma physics and electrodynamics, New York: Acid-free paper, 2009.

[15] R. McDaniel, "A Review of Equatorial Spread F," 1998.

[16] U.S. NAVAL RESEARCH Lab, "Plasma Physics Division," 25 March 2018. [Online]. Available: https://www.nrl.navy.mil/ppd/equatorial-spread.

[17] M.A Abdu et al, "Thermospheric meridional wind control of equatorial spread F and evening prereversal electric field," *Geophysical Research Letters,* vol. 33, no. 7, 2006.

[18] P. Rama Rao, "Characteristics of the Indian equatorial ionosphere," in *Characteristics of the Indian equatorial ionosphere*, Department of Physics, Andhra University, INDIA, 2006, p. 6.

[19] D.H Sharp et al, "An Overview of Rayleigh-Taylor Instability," *Physica D. 12: 3–18,* 1984.

[20] A.C Das, Space Plasma Physics: An Introduction, Narosa Publishing House, 2004, p. 107.

[21] J.F Cecile et al, "HF radar observations of equatorial spreadF over West Africa," *Annales Geophysicae, vol. 14,* p. pp. 411 – 418, 1996.

[22] C.Y Huang et al, "Equatorial plasma bubbles observed by DMSP satellites during a full solar cycle: Toward a global climatology," *Journal of Geophysical Research, vol.,* p. pp. 1 – 6, 2002.

[23] S.L Ossakow et al, Nonlinear equatorial spread F: Dependence on altitude of the F peak and bottomside background electron density gradient scale length, Geophys. Res., 84(A1), 17–29, doi:10.1029/JA084iA01p00017, 1979.

[24] M. Kelley, The Earth's Ionosphere, plasma physics and electrodynamics, San Diego: Elsevier Inc., 1989.

[25] S. Rungraengwajiake et al., "The variation of equatorial spread-F occurrences observed by ionosondes at Thailand longitude sector," *Advances in Space Research,* vol. 52, no. 10, pp. 1809-1819, 2013.

[26] S. Klinngam et al, "The statistics of equatorial spread-F at the conjugate stations in Southeast Asia,", The 4th Joint International Conference on Information and Communication Technology, Electronic and Electrical Engineering (JICTEE), Chiang Rai, 2014, pp. 1-5., 2014.

[27] S. Klinngam et al, "The statistics of equatorial spread-F at the conjugate stations in Southeast Asia," *Information and Communication Technology, Electronic and Electrical Engineering (JICTEE),* 2014.

[28] NOAA, "http://www.swpc.noaa.gov," 2018. [Online]. Available: http://www.swpc.noaa.gov/phenomena/f107-cm-radio-emissions. [Accessed 07 January 2018].

[29] L.A. McKinnell et al, "Predicting the probability of occurrence of spread-F," *Advances in Space Research 46,* p. 1047–1054, 2010.

[30] T. Yokoyama et al, "West wall structuring of equatorial plasma bubbles simulated by three-dimensional HIRB model.," *J Geophys Res Space Physics,* pp. 8810-8816, 2015.

[31] R.T Tsunoda et al, "Upwelling: A unit of disturbance in equatorial spread-F," *Progress in Earth and Planetary Science,* pp. DOI 10.1186/s40645-015-0038-5, 2015.

[32] N. Wolchover, 2018. [Online]. Available: https://www.quantamagazine.org/new-theory-cracks-open-the-black-box-of-deep-learning-20170921/.

[33] A. Karpathy, "CS231n Convolutional Neural Networks for Visual Recognition," 28 February 2018. [Online]. Available: http://cs231n.github.io/neural-networks-1/.

[34] F. Rosenblatt, "THE PERCEPTRON: A PROBABILISTIC MODEL FOR INFORMATIN STORAGE ORGANIZATION IN THE BRAIN," *Psychological Review,* pp. 387-408, 1958.

[35] L. Fausett, Fundamentals of Neural Networks: Architectures, Algorithms, and Applications, Prentice-Hall, 1994.

[36] dataaspirant, "Supervised and unsupercised learning," 28 Febrauary 2018. [Online]. Available: http://dataaspirant.com/2014/09/19/supervised-and-unsupervised-learning/.

[37] Hindayati Mustafidah et al, "Selection of Most Appropriate Backpropagation Training Algorithm in Data Pattern Recognition," *International Journal of Computer Trends and Technology (IJCTT),* pp. 92-95, 2014.

[38] S. Haykin, Neural Networks and Learning Machines (Third Edition), Ontario: Pearson Education, 2009.

[39] McKinnell et al, "Prediction of the probability of occurrence of spread-F over Brazil using neural networks," *37th COSPAR Scientific Assembly,* p. 1979, 2008.

[40] D. kriesel, A Brief Introduction to Neural Networks, Bonn: www.dkriesel.com, 2005.

[41] J.L. Mark Orr, Introduction to Radial Basis Function Networks, Edinburgh: Matlab, 1996.

[42] Yann LeCun et al, "Deep learning," pp. 436-444, 2015.

[43] Ilya Sutskever et al, "Generating Text with Recurrent Neural Networks," *International Conference on Machine Learning,* pp. 1017-1024, 2011.

[44] J.B Habarulema et al, "Prediction of global positioning system total electron content using Neural Network over South Africa," *Atmospheric and Solar-Terrestrial Physics,* pp. 1842-1850, 2007.

[45] L. M. J.B Habarulema, "Investigating the performance of neural network backpropagation algorithms for TEC estimations using South African GPS data," *Anales Geophysicae,* pp. doi:10.5194/angeo-30-857, 2012.

[46] T. Maruyama et al., "Ionospheric Irreguarlities and the SEALION Project; Outline of the SEALION Project and Initial Results," *Journal of the National Institute of Information and Communication Technology,* pp. 1-4, 2009.

[47] Fritts et al, "Overview and summary of the Spread F experiment (SpreadFEx)," *Annales Geophysicae,* vol. 27, no. 5, pp. 2141-2155, 2009.

[48] M. A. Abdu et al., "Equatorial spread F statistics in the American longitude: some problems relevant to ESF description in the IRI scheme," *Advances in Space Research,* vol. 25(1), pp. 113-124, 1999.

[49] L. (. W. S. Rayleigh, "Investigation of the character of the equilibrium of an incompressible heavy fluid of variable density," *Proceedings of the London Mathematical Society,* vol. 14, p. 170–177, 1883.

[50] D. a. S. E. Hysell, "Electrostatic plasma turbulence in the topside equatorial F region ionosphere," *Journal of Geophysical Research: Space Research,* 2002.

[51] A. Das, "Space Plasma Physics, an introduction," *Narosa Publishing House, New Delhi,* p. 107, 2004.

[52] S. Klinngam, "The occurrence of equatorial spread-F at conjugate stations in Southeast Asia," *Advances in Space Research,* vol. 55, no. 8, pp. 2139-2147, 2015.

AUTHOR BIOGRAPHY

Author: Mr. Phimmasone Thammavongsy

Degree: Master of Engineering

Date of Graduation: 2nd July 2018

Date of Birth: 4th September 1991

Place of Birth: Xiengkhouang province, Lao P.D.R

Undergraduate and Graduate Education:

Master of Engineering in Computing in Engineering Systems,

King Mongkut's Institute of Technology Ladkrabang, Bangkok, Thailand, 2018

Bachelor's degree in Telecommunication Engineering,

National University of Laos (NUOL), Vientiane capital, Laos, 2013

Major: Computing in Engineering Systems (International Program)

Presentations and Publications:

[1] P. Thammavongsy, P. Supnithi, S. Klinngam, W. Phakphisut, K. Hozumi, and T. Tsugawa, "Statistical Analysis of High Frequency Radio Parameters on St. Patrick's Day in Thailand", 5th IEECON, pp 1-4, 2017.

[2] P. Thammavongsy, P. Supnithi, W. Phakphisut, K. Hozumi, and T. Tsugawa, "A simple Neural Network Model Development for Spread-F Events in Chumphon, Thailand", RCCIE, 2017.